



universität
wien

DIPLOMARBEIT

Titel der Diplomarbeit

In-vivo and in silico studies of the receptor binding specificity of human rhinoviruses

angestrebter akademischer Grad

Magister der Naturwissenschaften (Mag. rer.nat.)

Verfasserin / Verfasser:	Christoph Weber
Matrikel-Nummer:	0307431
Studienrichtung /Studienzweig (lt. Studienblatt):	Genetik / Mikrobiologie
Betreuerin / Betreuer:	Univ.-Prof. Dr. Dieter Blaas

Wien, am 23.Juni 2009

Diese Diplomarbeit widme ich meiner lieben Mutter
Christine Weber,
welche mich zu diesem Studium motiviert
und
im Verlauf dessen auch immer unterstützt hat.

Table of contents

Abstract:	9
Zusammenfassung:	10
1. Introduction	11
Picornaviruses.....	11
Classification of Picornaviruses	11
Organization and expression of the genome.....	13
Virion structure.....	14
The Picornaviral life cycle.....	15
Rhinoviruses	16
Symptoms of rhinovirus infection and immune-response:.....	17
Classification of rhinoviruses:	18
Receptors:	18
ICAM-1:	19
LDL receptors:.....	21
Heparan sulfate:.....	23
2. Materials and Methods:	24
Tissue culture medium:	24
Cells:	24
Viruses:	25
Plasmid:	25
Preparation of competent E. coli: (MgCl ₂ Method).....	26
Heat shock transformation of E.Coli:	26
Plasmid preparation (MIDI):	26
Restriction digest:	27
Site directed mutagenesis (“round the horn”):	27
Phenol-Chloroform extraction of DNA:.....	30
<i>In-vitro</i> transcription:.....	30
LiCl ₂ precipitation of RNA:	30
Preparation of HeLa cells for transfection and MaTra transfection:	31
Transfection of viral RNA with Lipofectamine2000:	31
Preparation of [³⁵ S]-radio labeled virus.....	31
Preparation of Staphylococcus aureus cells.....	32

Immune precipitation of the radiolabelled samples.....	32
Site directed mutagenesis (quick change)	33
Reverse transcription of Virus RNA	34
Amplification of the cDNA	35
Virus infection assay	36
Primer list:	36
Objectives:.....	38
3. Predictive bioinformatic identification of minor receptor group human rhinoviruses.....	39
3.1 Introduction:	39
3.2 Details of the rhinovirus – VLDL-receptor interaction:	39
3.3 Workflow of the method:	41
3.4 Modelling and evaluation of VP1 structures	41
3.5 Evaluating the result of the homology modelled VP1 structures:	42
3.6 Modelling VP1-VP1* -V3	44
3.7 Energy calculations.....	46
3.8 Result of the energy calculations.....	47
3.9 Correction of calculated affinities:	49
3.10 Evaluation of the results:	51
3.11 Different contribution of amino acid residues to the binding energy:.....	52
4. Binding energies between HRVs and LDLR module 5 (L5) of human and mouse.....	59
4.1 Result of the Fastcontact calculations:	61
5. Bioinformatic analysis of the field isolated rhinoviruses:.....	63
5.1 Introduction:	63
5.2 Bioinformatic affinity calculations:.....	64
5.3 Results of the affinity calculations:	65
5.4 Detection of binding abilities of the field isolated viruses:	68
6. Mutational analysis of a major group human rhinovirus.	69
6.1 PCR mutagenesis “round the horn”-method	70
6.2 <i>In-vitro</i> transcription of HRV14_HI2 RNA and transfection of HeLa cells.	71
6.3 Immunoprecipitation of [³⁵ S] labeled samples	72
6.4 PCR mutagenesis “quick change”	73
6.5 RNA transcription and transfection of Hela cells.....	74
6.6 Screening the chimeric viruses via RT-PCR.....	74
6.7 Infection assay	75

7. Discussion:	76
Bioinformatics:	76
Analysis of the unclassified field isolates.....	78
Mutagenesis:	79
References	81
Acknowledgement:.....	85
Curriculum vitae.....	87

Abstract:

Major group HRVs bind intercellular adhesion molecule 1 (ICAM1) and minor group HRVs bind members of the low-density lipoprotein receptor (LDLR) family for cell entry. Whereas the former share common sequence motives in their capsid proteins, in the latter only a lysine residue within the binding epitope in VP1 is conserved; this lysine is also present in ten "K-type" major group HRVs which fail to bind LDLR.

A bioinformatic approach based on the available VP1 sequences three-dimensional models of VP1 of all HRVs were built and binding energies, with respect to module 3 of the very-low density lipoprotein receptor, were calculated. Based on the predicted affinities, K-type HRVs and minor group HRVs were correctly classified. With the intention to find conserved binding patterns the energy tables that indicate the interacting binding partners were transformed into heatmaps. In addition to the heatmaps a bar diagram that shows the interaction energy of the different receptor residues of all minor group and K-type viruses was made. In further improvements the module 3 of VLDLR was replaced by the ligand binding repeat 5 of human and mouse LDLR. To examine the predictive power of the *in silico* application two non-classified field isolates were analyzed. In a site directed mutagenesis experiment the HI-loop of HRV14 (major group) was changed into the sequence of the HI-loop of HRV2 (minor group). The newly created chimeric virus (HRV14_HI2) was not infective. Also a revision of the experiments under optimized conditions could not create an infective virus. The only chimeric virus that could be produced was HRV14_K. In this virus a histidine to lysine mutation at position 232 was successfully accomplished. The properties of this artificial K-Type virus to bind LDLR were checked in infection assays using RD cells.

Zusammenfassung:

Humane Rhinoviren (HRV) sind verantwortlich für rund die Hälfte aller Erkältungen beim Menschen. Die zur Familie der Picornaviren gehörigen Rhinoviren besitzen ein ikosaedrisches Kapsid, das aus den 4 viralen Strukturproteinen (VP1, VP2, VP3 und VP4) aufgebaut ist. Der Durchmesser dieses Kapsids beträgt 30 nm. Die mehr als hundert verschiedenen Virustypen können anhand ihrer Fähigkeit an zelluläre Rezeptoren zu binden eingeteilt werden. Die weitaus größere Gruppe der beschriebenen Rhinoviren binden an den ICAM-1 Rezeptor um in die Wirtszelle zu gelangen. Eine kleine Gruppe von Rhinoviren, genannt „minor group“ Viren binden an LDL-Rezeptoren, wie LDLR, LRP und VLDLR. Ein Ziel dieser Arbeit war es neue Einblicke in die Details der Interaktion von Virus und Rezeptor zu erhalten. Vorhergehende Untersuchungen dieser Interaktion zeigten, dass nur ein virales Protein in diese Wechselwirkung involviert ist. Dieses virale Protein 1 (VP1 genannt), und im speziellen die Oberflächen-„loops“ sind an der Wechselwirkung mit den LDL Rezeptoren beteiligt. Sequenzanalysen der LDLR bindenden Rhinoviren („minor group“ viruses) zeigten, dass lediglich ein Aminosäurerest, ein Lysin, strikt konserviert ist. Dieses Lysin befindet sich in der Mitte des HI-„loop“. Man nahm an, dass dieses Lysin verantwortlich sei für die Bindung an LDL Rezeptoren. Es wurden jedoch einige Rhinovirus Typen gefunden, die an der gleichen Stelle ebenfalls ein Lysin aufweisen. Diese Gruppe von Viren (K-Typen) können anhand ihrer Sequenzmerkmale nicht von „minor group“ Viren unterschieden werden, jedoch können sie den LDL Rezeptor nicht für die Infektion verwenden.

Im ersten Teil meiner Diplomarbeit ging es um die Entwicklung eines Bioinformatischen Klassifizierungsverfahrens. Mit diesem sollte es möglich sein alle bekannten Rhinovirus Typen gemäß ihrer Rezeptor Spezifikation einzuteilen. Die Methode beruht auf der Hypothese, dass bindende Typen eine zum Rezeptor komplementäre Ladungsverteilung an ihrer Oberfläche aufweisen, die es ihnen ermöglicht den Rezeptor zu binden. Gemäß dieser Hypothese sollten die Bindungsaffinitäten der bindenden Typen höher sein als die der nicht bindenden Typen. Die 3D Strukturen des VP1 Proteins wurden durch „homology modelling“ erhalten. 3D Koordinaten, die der determinierten Röntgenstruktur von HRV2 mit gebundenen V3 entnommen wurden, dienten als Matrize für alle die Anordnung aller anderen Rhinoviren-Rezeptor Komplexe. Nach einem Energie Minimierungsschritt wurden die Modelle aller Rhinoviren mit gebundenem Rezeptor hinsichtlich ihrer Bindungsaffinität analysiert. Eine der verwendeten Methoden, war tatsächlich in der Lage alle Rhinoviren korrekt zu klassifizieren. Die Gruppe der K-Typen hatten generell höhere Affinitäten zu dem verwendeten Rezeptor (V3), als andere „major group“ Viren.

Im anschließenden Teil der Arbeit wurde ein „major group“ Virus (HRV14) so mutiert, das er einen gänzlich veränderten HI-loop aufweist. Die Sequenz des am stärksten in der Virus-Rezeptor Interaktion involvierten Oberflächen“loop“ (HI-loop) wurde gegen die Sequenz eines „minor group“ Virus mittels Zielgerichteter Mutagenese ausgetauscht. RNA Klone der mutierten Sequenz waren jedoch nicht infektiös. Es gelang lediglich einen infektiösen Klon der nur eine Punktmutation im HI-„loop“ aufwies herzustellen.

1.Introduction

Picornaviruses

Members of the family Picornaviridae (pico=small) share icosahedral structural symmetry and a genome of single-stranded RNA of positive sense. Because of the positive polarity the RNA can directly be used as template for synthesis of all the viral proteins required for viral replication, and thus picornavirus RNA is infectious. The first infectious cDNA clone of a RNA virus was that of poliovirus [1]. Generally, picornaviruses have played an important role in modern virology. All members of this family lack a lipid envelope and are therefore resistant to ether, chloroform and alcohol. Within this family we can find some important human and animal pathogens, including poliovirus, hepatitis A, rhinovirus and FMDV (food and mouth disease virus).

Classification of Picornaviruses

The family Picornaviridae belongs to the order Picornavirales and consists of 8 genera: Enterovirus, Cardiovirus, Aphthovirus, Hepatovirus, Parechovirus, Erbovirus, Kobuvirus and Teschovirus, plus three proposed genera named "Sapelovirus", "Senecavirus" and "Tremovirus". (Fig.1)

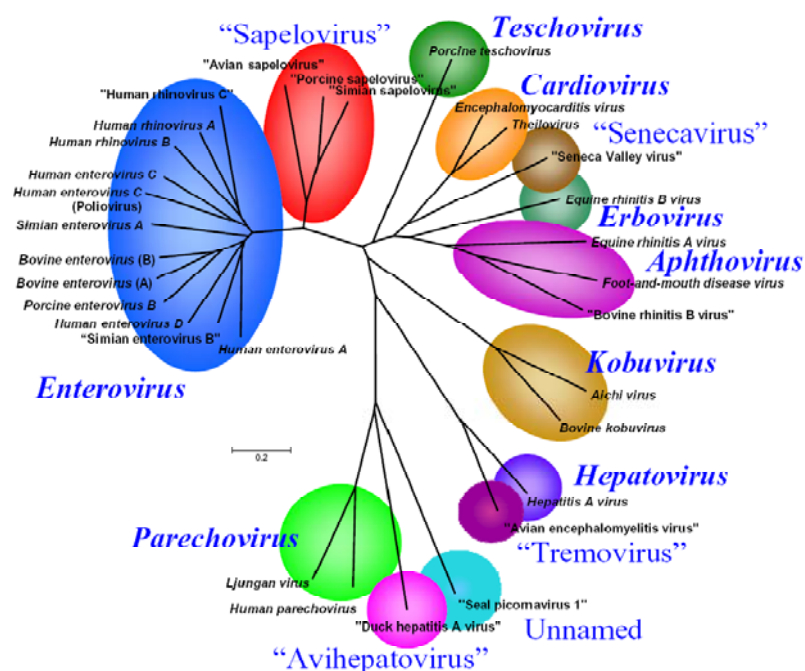


Figure 1: Unrooted neighbor-joining tree of Picornaviridae based on a comparison of the P1 capsid region. (http://www.picornastudygroup.com/posters/psg_posters.htm)

A list of important members of the picornavirus family can be seen in Table 1. Five of the picornaviridae genera contain human pathogens.

Genus/members	Virus name abbreviation ^a	Usual host(s)	Transmission	Disease	World distribution
Enterovirus					
Poliovirus (3)	PV	Humans	Oral/fecal, contact	Paralysis, aseptic meningitis	Originally worldwide, extirpated in Americas
Echovirus (29)		Humans	Oral/fecal, contact	Aseptic meningitis, paralysis, encephalitis	Worldwide
Coxsackie (23A and 6B)		Humans	Oral/fecal, contact	Common cold, myocarditis	Worldwide
Enterovirus (4 human, 30 other)		Humans, cattle, monkeys, swine	Oral/fecal, contact	Aseptic meningitis, conjunctivitis (type 70)	Worldwide
Human rhinoviruses (>100 serotypes)	HRV-A, HRV-B, HRV-C	Humans	Aerosols, contact	Common cold	Worldwide
Parvovirus					
Human parvovirus (formerly echovirus 22)	HPeV	Humans	Oral/fecal	Gastroenteritis	Worldwide
Aphthovirus					
Foot-and-mouth disease	FMDV	Cattle, swine	Oral/fecal, contact	Lesions on mouth and feet	Worldwide (except U.S.)
Cardiovirus					
Encephalomyocarditis	EMCV	Mice	Oral/fecal, contact	Encephalitis, myocarditis	Worldwide
Kobuvirus					
Aichi	AiV	Humans	Oral/fecal	Gastroenteritis	Isolated in Japan (oysters)
Hepatovirus					
Hepatitis A	HAV	Humans	Oral/fecal	Hepatitis	Endemic worldwide
Teschovirus					
Porcine teschovirus (formerly porcine enterovirus 1 or PEV-1)	PTV	Swine	Oral/fecal	Paralysis, porcine encephalomyelitis	Britain, Central and Eastern Europe
Erbovirus					
Equine rhinotracheitis B	ERBV	Horses	?	?	?

Table 1: All genera of the picornavirus family with their usual hosts, mode of transmission and caused diseases. Table modified from the book, James, S. & Allen, S. (2001). *Viruses and Human Disease*. US: Academic Press.

Rhinoviruses are very similar to enteroviruses but they can be distinguished by physical properties, genome organization and different symptoms of the diseases they cause. As the name implies, enteroviruses can replicate in the alimentary tract and are resistant to low pH. This genus contains some important human pathogens like Poliovirus, Coxsackievirus, Echovirus, Human Enterovirus and many other non human enteric viruses. Rhinoviruses are labile at $\text{pH} \leq 3.0$ but many are already inactivated at a much higher pH; this acid lability plays a role in uncoating of viral RNA.

Properties of Rhino- and Entero-viruses						
	pH sensitivity	Optimum growth temperature	Detergent sensitivity	Serotypes	Transmission	Site of primary infection
Rhino viruses	labile to acid pH	~ 33 °C		>100	aerosol	upper respiratory tract
Entero viruses	resistant to acid pH	~ 37 °C	resistant	72	oral-fecal	gut

Table 2: Properties of rhinoviruses and enteroviruses taken from <http://pathmicro.med.sc.edu/virol/picorna.htm>.

Organization and expression of the genome

The picornaviral genome is a single stranded RNA molecule of about 8 kb (6.5 to 9.5 kb). It contains one open reading frame (ORF) and is translated into a single polyprotein. This polyprotein (~2200 amino acids) is cleaved by two virus-encoded proteinases to form different polypeptides. The polypeptide can be divided into three regions P1, P2 and P3. The cleavage product P1 consists of a polyprotein precursor for the four structural proteins of the virus, VP1–4. P1 is first cleaved in trans to VP0, VP1, and VP3 by 3CDpro. VP0 is later cleaved to VP2 and VP4 during virus assembly.

The P2 and P3 region encode non-structural proteins that are important for the co-translational cleavage of the polyprotein (viral proteases 2A and 3C), inhibition of host cell functions (proteases 2A, 3C and Leader protease), determination of host range (2B,2C) and replication of the viral RNA (2C, 3AB, Vpg and RNA polymerase 3D).

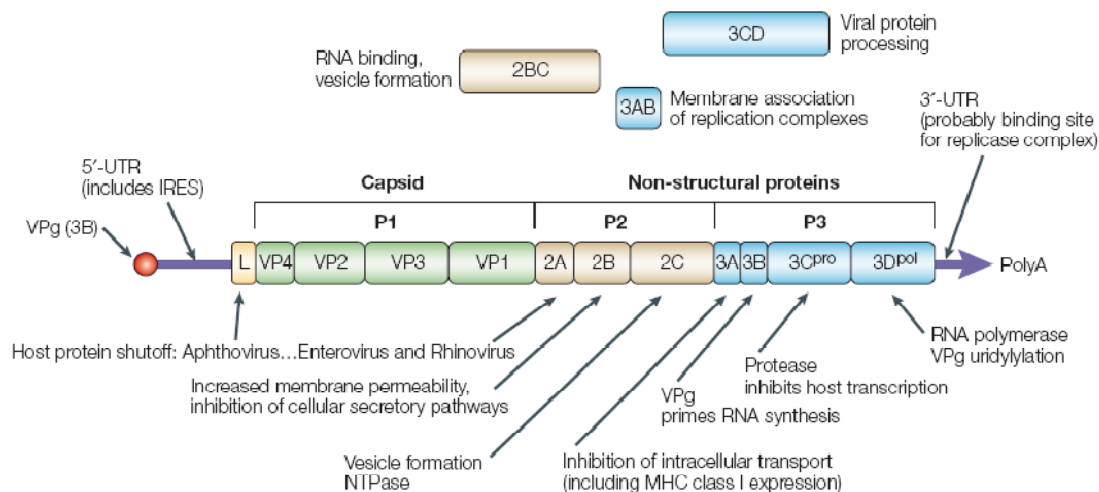


Figure 2 A typical picornaviral genome with the 3 main cleavage intermediates (P1, P2, P3). Also the functions of the 12 major polypeptides are shown. IRES, internal ribosomal entry site; UTR, untranslated region; Vpg, viral protein genome-linked. Picture taken from Ref. [2]

The picornaviral genome contains a small protein, VPg, covalently bound to the 5' end, which is the primer for initiation of RNA synthesis. VPg is normally removed from the RNA by a cellular enzyme, but its removal is not required for its translation. The 3' end of the RNA is polyadenylated. The 5' nontranslated region of a picornaviral RNA possesses an IRES (internal ribosome entry site) therefore the RNA is translated by a cap-independent mechanism. To promote the translation of the viral mRNA, rhinoviruses (and other picornaviruses) inhibit cap-dependent translation by cleavage of the cap binding protein eIF4G (eukaryotic initiation factor 4G) by the viral protease 2A^{pro}.

Virion structure

Picornaviruses are spherical in shape, with a diameter of 30 nm. The particles are composed of a protein shell that surrounds the naked RNA. The particles are non-enveloped and are composed of 60 copies of the 4 structural proteins VP1, VP2, VP3 and VP4 arranged as 12 pentamers forming an icosahedron. The capsid is responsible for specific binding to cell surface receptors.

Genus	Leader protein	Representative species	Receptor	Disease(s)	Natural host
Enterovirus	No	Poliovirus	CD155	Poliomyelitis	Human
Enterovirus	No	Coxsackievirus	CAR, DAF	Myocarditis, pancreatitis, meningitis	Human
Enterovirus	No	Rhinovirus	ICAM-1, LDLR	Common cold	Human
Cardiovirus	Yes	Theiler's murine encephalomyelitis virus	?	Encephalomyelitis	Mouse
Aphthovirus	Yes	Foot-and-mouth-disease virus	Integrins	Foot-and-mouth disease	Cloven-hooved ungulates
Erbovirus	Yes	Equine rhinitis B virus	?	Acute respiratory disease	Horses
Kobuvirus	Yes	Aichi virus	?	Gastroenteritis	Human
Teschovirus	Yes	Porcine teschovirus	?	Encephalomyelitis	Pigs
Hepatovirus	No	Hepatitis A virus	HAVcr-1	Hepatitis	Human
Parechovirus	No	Human parechovirus	Integrins	Gastroenteritis, respiratory disease	Human

CAR, coxsackievirus and adenovirus receptor; DAF, decay accelerating factor ; ICAM-1, intracellular adhesion molecule 1; LDLR, low-density-lipoprotein receptor.

Figure 3: Examples of picornaviruses and their receptors used for cell entry. Picture modified from Ref. [2].

The shell is formed by VP1 to VP3, and VP4 is completely inside. VP1, VP2, and VP3 have no sequence homology, yet all three proteins have a similar conformation: they form an eight-stranded, antiparallel β -barrel (also called a β -barrel jelly roll or a Swiss-roll β -barrel). This domain is a wedge-shaped structure made up of two antiparallel β -sheets (see. Fig.4). One β -sheet forms the wall of the wedge, and the second, which has a bend in the center, forms both

a wall and the floor. The wedge-shape facilitates the packing of structural units to form a dense, rigid protein shell.

The main structural differences among VP1, VP2, and VP3 lie in the loops that connect the β -strands and the N- and C-terminal sequences that extend from the β -barrel domain. These amino acid sequences give each picornavirus its distinct morphology and antigenicity. The C-termini are located on the surface of the virion, and the N-termini are on the interior.

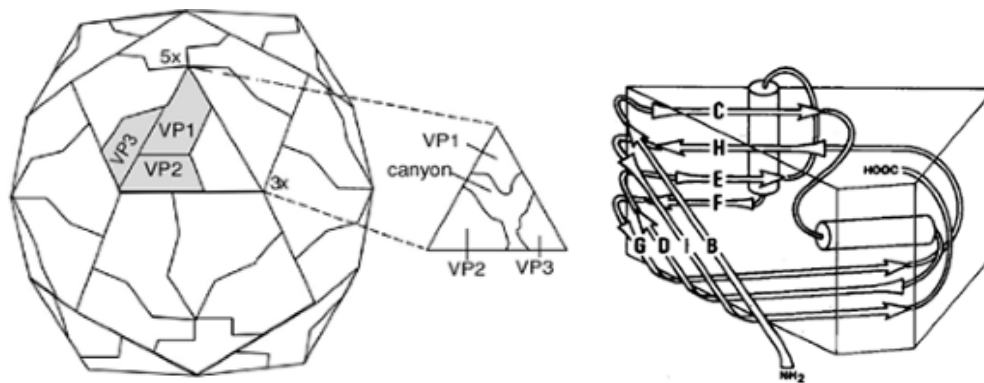


Figure 4: Left panel: Schematic of the picornavirus capsid, showing the pseudoequivalent packing arrangement of VP1, VP2, and VP3. Picture taken from Ref. [3]. Right panel: The typical folding of the capsid proteins (2 antiparallel β -sheets). <http://www.med.uni-jena.de/virologie/zell/lehre/picornaviren/picornaviren.html>

The Picornaviral life cycle

The life cycle of picornaviruses is shown in Figure 5. Attachment to cellular receptors (LDL-R or ICAM-1 for rhinoviruses), is the first step. The second step is the internalization of the virion by receptor mediated endocytosis. During internalization uncoating takes place. The result of this uncoating is the release of viral RNA to the cytoplasm of the host cell. The viral RNA can serve directly as a template for protein synthesis. The protein synthesis is initiated in a cap-independent manner, via an IRES sequence located at the 5' end of the genome. The polyprotein is processed via protease cleavage to the different virus proteins. Some of them help to form the viral replication complex. During replication, a full-length complementary copy of the genomic RNA is produced that serves as a template for the synthesis of genomic RNA. This complementary RNA template is called minus-strand RNA (-). Much more (+)RNA than (-)RNA is produced, since (+)RNA is needed for translation and encapsidation

into progeny as well as for replication, whereas (-)RNA is needed only as a template for making (+)RNA.

The RNA-dependent RNA polymerase 3Dpol is strictly primer dependent. In the presence of template, 3Dpol can uridylylate VPg on a specific tyrosine residue. This nucleotidyl peptide then functions as a primer for the initiation of RNA synthesis. The last steps are virus packaging and viral egress.

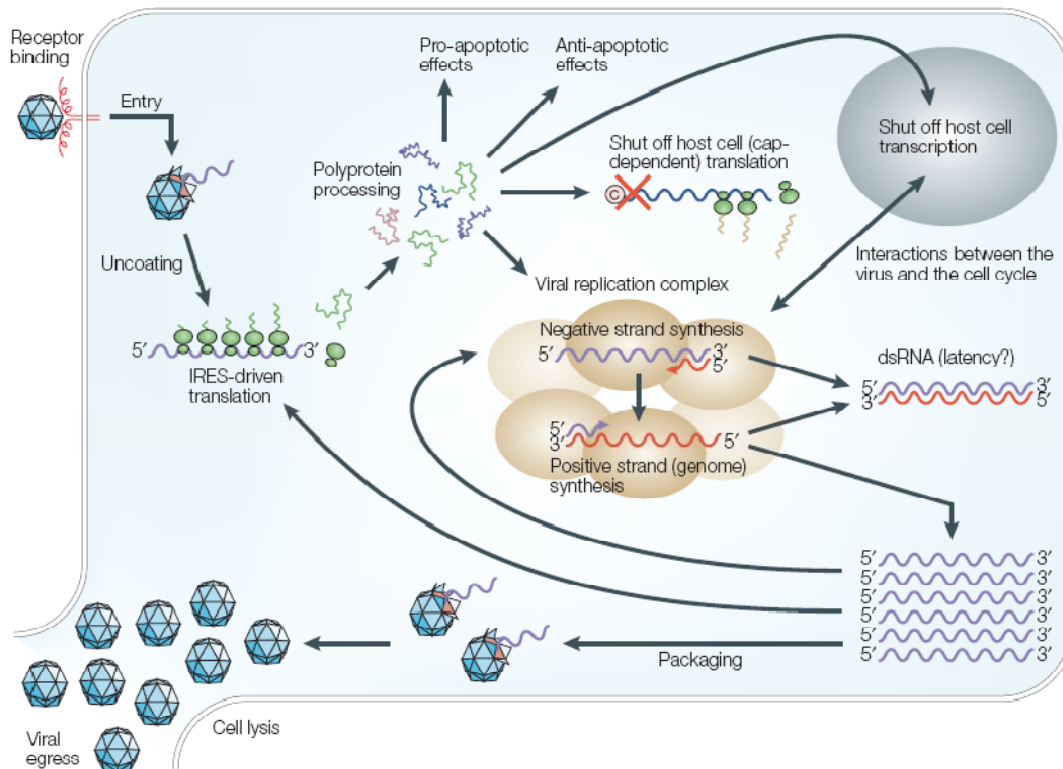


Figure 5: A picornaviral life cycle. The main events of infection are described in the text. (+) stranded RNA is shown in blue, (-)-stranded RNA is shown in red. Picture taken from Reference [2].

Rhinoviruses

Human rhinoviruses (HRV) are responsible for nearly 50% of all common cold infections. Their name (Rhinos = nose) reflects the primary site of infection. Since the discovery of rhinovirus in 1956 [4] [5], more than 100 serotypes have been identified.

HRVs are the largest genus within the picornavirus family. The human rhinoviruses are non enveloped viruses with a positive single strand RNA genome (7500bp). The capsid is an icosahedron, which is composed of 60 copies of each of the four viral proteins (VP1-VP4). The diameter of this T=1 pseudo T=3 capsid is 30nm. Rhinoviruses replicate predominantly

in the upper respiratory tract and are transmitted by direct person-to-person contact. Recently studies revealed that rhinoviruses are also able to replicate in lung tissue [6]. Coughing and sneezing, common syndromes of rhinovirus infections help spreading the virus. The development of an effective vaccine and antiviral prophylaxis against HRV is hampered by the extensive antigenic diversity.

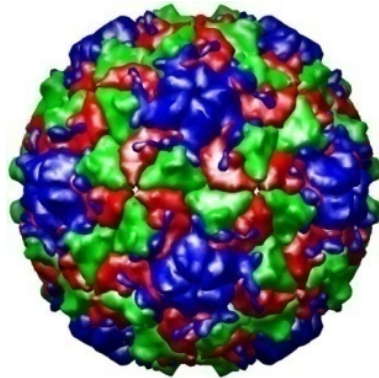


Figure 6: Icosahedral surface of HRV2 (pdb code: 1fjn) composed of the four viral proteins: VP1 colored in blue; VP2 colored in red; VP3 colored in green; VP4 is inside. Picture was made with UCSF Chimera [7] using the multi-scale model function.

Symptoms of rhinovirus infection and immune-response:

The symptoms of a rhinovirus infection are discharging or blocked nasal passages often accompanied by sneezes, a sore throat, rhinorrhea, and general malaise. The symptoms occur from 1 to 4 days after infection at which time extremely high titers of the rhinovirus are found in the nose. The symptoms experienced depend on the number of virus particles replicated. Infected cells produce a variety of molecules, such as histamine that result in increased nasal secretions. It is the production of such molecules rather than direct cellular destruction that accounts for the symptoms experienced by the patient. The primary infection results in the production of IgA in nasal secretions and IgG in the bloodstream. Since rhinoviruses do not enter the circulation, the mucosal IgA response is the most important. This leads to immunity and resolution of the disease although the levels of nasal IgA decrease rapidly. Immunity against a particular serotype may last 1 to 2 years. Interferon production is the primary means of defense, preceding the antibody response. Many infected persons (about 50%) do not show symptoms of a rhinovirus infection but are nevertheless capable of passing on the

infection. Although the lower respiratory tract is usually not affected, bronchopneumonia can occur in rhinovirus infections, particularly in children <http://pathmicro.med.sc.edu/virol/rhino.htm>.

Even more important than causing common colds, rhinoviruses also trigger the great majority of asthma exacerbations [8]. Rhinovirus infection has also been associated with nearly half of all chronic obstructive pulmonary disease (COPD) exacerbations [9].

Classification of rhinoviruses:

HRVs can be classified according to their amino acid-sequence similarity. Phylogenetic analysis of the capsid protein VP1 coding sequences of all 102 human rhinovirus (HRV) strains revealed two major genetic clusters. According to this, rhinoviruses are divided in A and B species. This classification correlates with the sensibility of rhinoviruses to antiviral compounds. Rhinoviruses A (HRVA) comprise 73 Serotypes. The average amino acid identity within the class of HRV A is 78% (range 68%-95%). Amino acid identity within HRV B is 83% (range 75%-99%) [10].

Based on receptor binding properties, rhinoviruses can be divided into 2 classes. The one class of rhinoviruses binds to ICAM-1 (intercellular adhesion molecule 1). The others bind to members of the LDL (low density lipoprotein)-receptor family.

Recently, a number of sequences with high similarity to the genomes of HRVs have been detected in patients. These rhinovirus types have not been cultured, but their sequences indicated that they are a third species called HRV-C. [11-13].

Receptors:

Based on their receptor use, two groups of HRV can be distinguished. Major group viruses use intercellular adhesion molecule-1 (ICAM-1) as their receptor [14]. The 12 minor group viruses attach to low density lipoprotein (LDL) receptor, very-LDL (VLDL) receptor, and LDLR-related protein on the cells [15,16].

ICAM-1:

ICAM-1 belongs to a family of transmembrane, glycoprotein cell adhesion molecules whose extracellular part is composed of five immunoglobulin Ig domains. The normal function of human intercellular adhesion molecule-1 (ICAM-1) is to provide adhesion between endothelial cells and leukocytes after injury or stress. This plays a major role in the migration of leukocytes from the blood to sites of inflammation.

During an inflammatory response, expression of ICAM-1 in endothelial cells is greatly increased. Thus, these cells become “sticky” to leukocytes in the circulating blood. This is followed by migration of leukocytes to the sites of injury or infection.

1A	17	34	51	68	85
1B	18	35	52	69	86
2	19	36	53	70	87
3	20	37	54	71	88
4	21	38	55	72	89
5	22	39	56	73	90
6	23	40	57	74	91
7	24	41	58	75	92
8	25	42	59	76	93
9	26	43	60	77	94
10	27	44	61	78	95
11	28	45	62	79	96
12	29	46	63	80	97
13	30	47	64	81	98
14	31	48	65	82	99
15	32	49	66	83	100
16	33	50	67	84	HANKS

Table 3: Classification table of human rhinoviruses. HRV A species that are classified into the major group are colored in red, minor group viruses are colored in blue and “K-types” are colored in green. HRV B species are represented in bold. HRV87 in white was re-classified as enterovirus 68.

The normal ligands of ICAM-1 are leukocyte function-associated antigen or macrophage-1 antigen [17] (Fig.7).

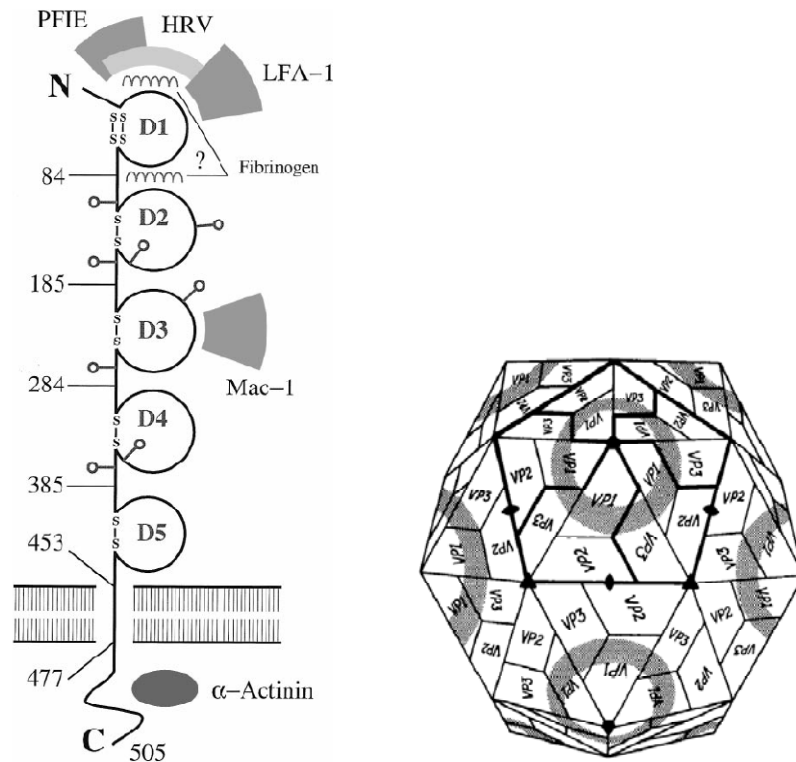


Figure 7 left: Structure of ICAM-1 with the different ligand binding sites and glycosylation sites (lollipop shaped structures) PFIE...*Plasmodium falciparum* infected erythrocytes, LFA-1... leukocyte function-associated antigen 1, Mac-1... macrophage-1 antigen right: A major group human rhinovirus showing the binding-site (canyon) of ICAM-1 (gray ring). Pictures taken from Ref. [18].

The ICAM-1 binding site of major group viruses is located at a surface depression around the fivefold axes, the so-called canyon, which is a highly conserved structural feature among HRVs [19,20]. The canyon is composed of the north wall (built by VP1) around the fivefold axis and the south wall (built mainly by VP2 and VP3). While the most accessible residues along the canyon walls are hypervariable, the less exposed residues in the canyon floor are conserved and used for receptor binding; this has been thought to be a strategy allowing the virus to escape antibody neutralization [21]. However, it was demonstrated that antibodies can also access the canyon [22]. There is a hydrophobic pocket in VP1 directly underneath the canyon floor. This pocket is usually filled with a fatty acid (pocket factor), which stabilizes

the virion during its cell-to-cell transit [23]. Hydrophobic antiviral compounds (e.g. the WIN compounds) were found to bind to the VP1 pocket and to inhibit capsid breathing.

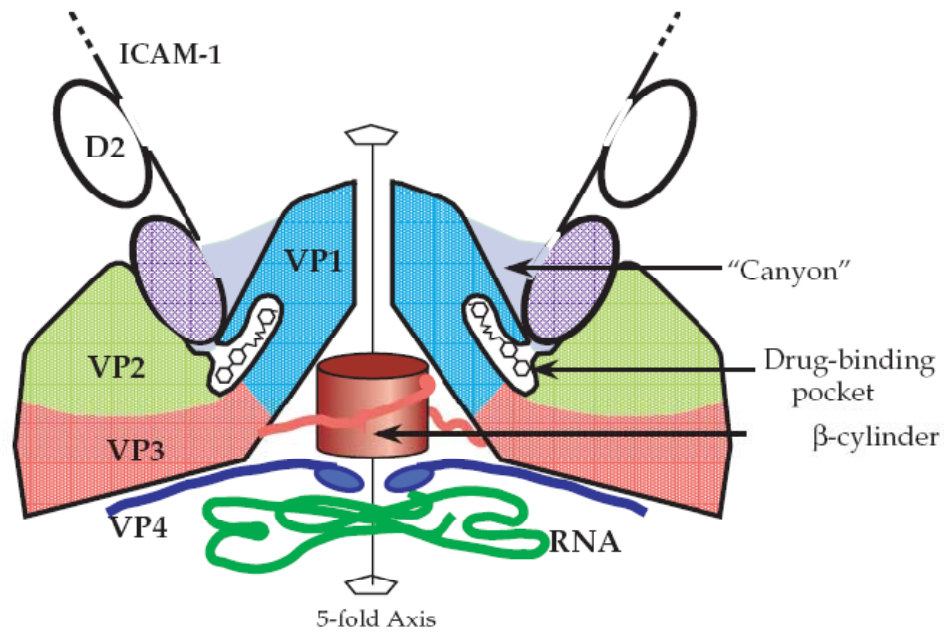


Figure 8: Binding of a major group rhinovirus to ICAM-1. Only the 2 distal domains of ICAM-1 are presented. Picture taken from the book, James, S. & Allen, S. (2001). *Viruses and Human Disease*. US: Academic Press.

LDL receptors:

The members of the LDL receptor family are structurally related endocytic receptors. The LDL receptor family members are able to bind and internalize a plethora of ligands; as a consequence, they play important roles in diverse physiological processes. These receptors are key players in the lipoprotein metabolism, vitamin homeostasis, Ca²⁺ homeostasis, cell migration, and embryonic development [24]. A structural overview of members of the LDLR-family that can serve as receptors for minor group viruses can be seen in Fig.9. Members of the low-density lipoprotein receptor family possess various numbers of ligand binding repeats that non-equally contribute to binding of minor group human rhinoviruses [25].

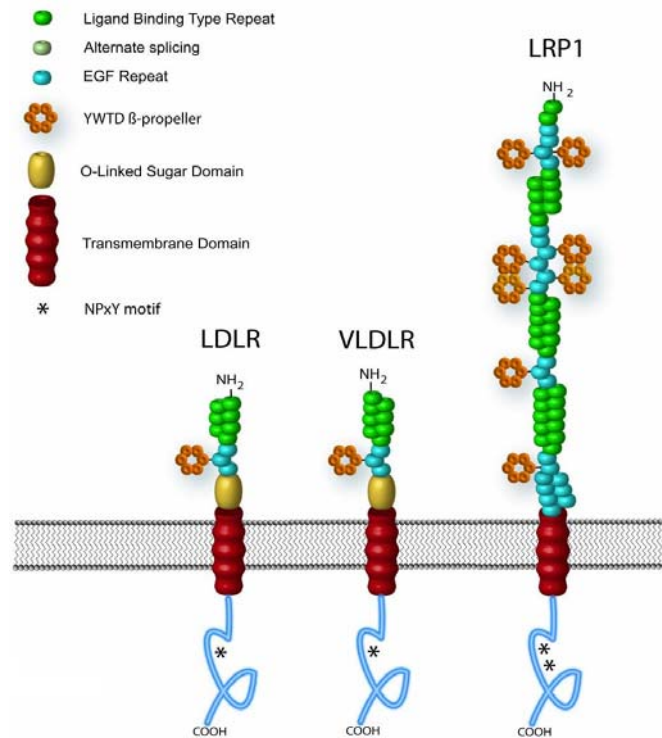


Figure 9: 3 members of the LDL-receptor family that are used for cell attachment of minor group viruses. Picture taken from Reference [26].

The ligand binding domains of LDLR-family members are composed of different numbers of ligand binding repeats. In LDLR 7, VLDLR 8 and in LRP 31 ligand binding repeats are present. The regions of ligand binding repeats in LDLR, VLDLR and LRP are followed by 3 regions that are similar to epidermal growth factor precursor (EGF repeats). These repeats are containing YWTD motives that form a 6 bladed β-propeller. In LDLR and VLDLR an O-glycosylation region is present proximal to the transmembrane domain. In the cytoplasmic domain a NPXY internalization motive is present.

The attachment site on minor group viruses is located at the tip of the five-fold axis, at a star shaped dome, that is build by the loops of VP1. The receptor binding site of minor group viruses encompasses only VP1, whereas the binding site (canyon) of ICAM-1 encompasses VP1, VP2 and VP3 (Fig.10).

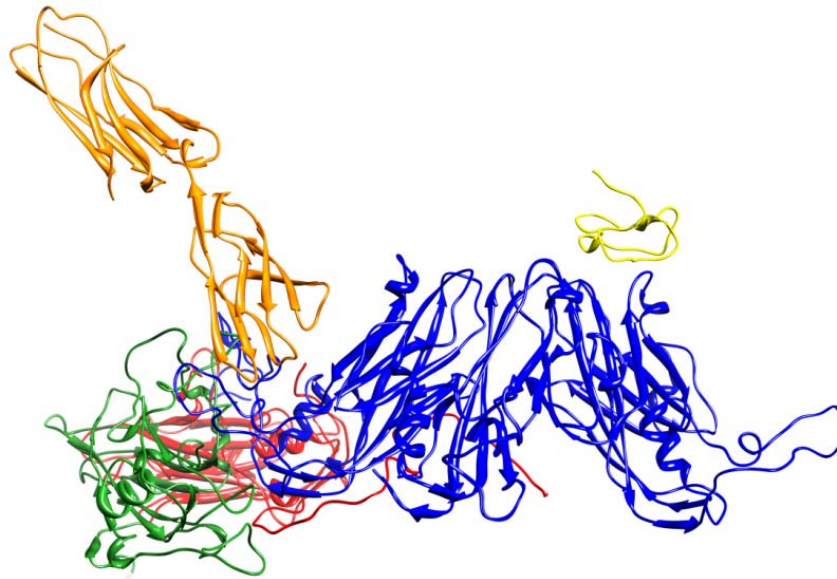


Figure 10: Binding sites of 2 different rhinovirus receptors. VP1 colored in blue VP2 colored in green, VP3 colored in red. The ligand binding repeat 3 of VLDLR is colored in yellow. The 2 distal domains of ICAM-1 are colored in orange.

Heparan sulfate:

The biological functions of heparin sulfate are cell adhesion, migration proliferation and differentiation [27]. Heparan sulfate is ubiquitously expressed at the surface of mammalian cells. It is characterized by a linear chain of 50-200 disaccharide units of beta-D-glucosamine (GlcN) 1-4 linked to beta-D-glucuronic acid. Recently, studies on HRV54 carried out by Khan [28] showed that this virus type is able to attach to cells via heparin sulfate. HRV54, a major group virus, was able to infect human rhabdomyosarcoma (RD) cells lacking ICAM-1. The infection could not be blocked with a recombinant soluble concatemer of VLDLR repeat 3 (MBP-V33333). Previously, it was shown that also variants of HRV89 are able to use heparin sulfate as a receptor for cell-entry. The interaction between HS and virus is basically an ionic interaction. A typical HS binding motive is BBXB or BBBXXB (B basic residue; X every residue). Such a motive was found in the VP1 of HRV54 but it is not clear whether it is indeed involved in HS attachment.

2. Materials and Methods:

Tissue culture medium:

MEM (Minimal Essential Medium, Gibco) for cultivating HeLa cells.

DMEM (Dulbecco's Modified Eagle Medium, Gibco) for cultivating RD and RD-ICAM cells.

Opti-MEM I (Gibco) for MaTra RNA transfection.

Growth medium: 10% heat inactivated fetal calf serum (hiFCS, Gibco) ; 1% Penstrep (Penicillin/Streptomycin, Gibco) ; 1% L-glutamine (Gibco)

Infection medium: 2% hiFCS ; 1% Penstrep ; 1% L-glutamine; 30 mM MgCl₂

Cells:

Cells were cultivated at 37°C in 5% CO₂ atmosphere.

For infection, 34°C in 5% CO₂ atmosphere.

Culturing, Splitting and Seeding of the Cells

Cells stored in liquid nitrogen in freezing medium (10% DMSO in FCS) were thawed and transferred to pre-warmed growth medium. Cells were centrifuged to remove DMSO. The cell were taken up in growth medium and shifted into 75 cm² cell culture flasks (CORNING lifescience). When the cell had reached 100% confluence they were washed with PBS and splitted using trypsin-EDTA (PAA). The detached cells were resuspended in growth medium and a required number of cells were transferred to respective plates. An aliquot of about 1/10 of the flask volume was used to keep the cells in culture.

HeLa (Ohio) cells:

Human cervical epithelial tumor cell line was obtained from *European Collection of Cell Cultures (ECACC)*.

Rhabdomyosarcoma (RD) cells:

Human muscle fibroblasts wild type (RD) provided by Dr. Darren S. Shaffren *New Castle Australia*

RD-ICAM cells:

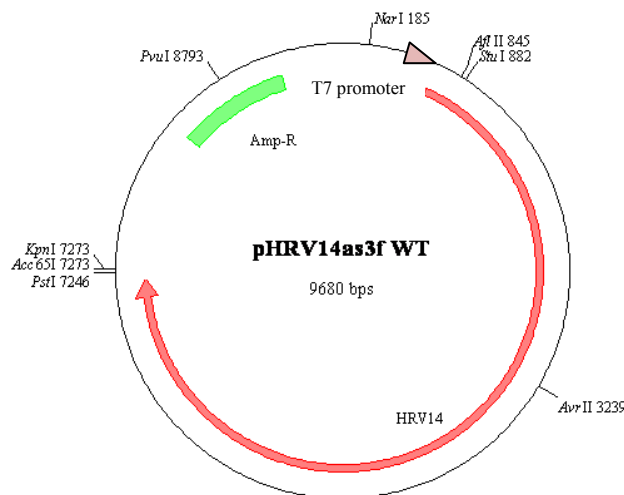
Human muscle fibroblasts transfected with human intercellular adhesion molecule-1 (RD-ICAM). Kindly provided by Dr. Darren S. Shaffren *New Castle Australia*

Viruses:

HRV2 and HRV14 viruses were originally obtained from ATCC.

Plasmid:

The plasmid pHRV14as3fWT was created by Tim Skern and was published in [29]. It contains the full cDNA genome of HRV14 embedded in the T7 cloning vector pSP72 (Promega). The most important feature of this plasmid is its T7 promoter. That makes it possible to obtain infectious + stranded RNA from this vector.



Preparation of competent E. coli: (MgCl₂ Method)

An o/n culture of Top10 E.coli cells was inoculated into 200 ml LB medium. The cells were grown at 37°C till an O.D. 0.4-0.5 was reached. Then the cells were harvested in sterile Falcon® tubes at 4000 rpm 5 min at 4°C. The cells were resuspended in 25 ml ice-cold 0.1M CaCl₂. After 25 min on ice the suspension was centrifuged again. (4000 rpm, 5 min). Cells were resuspended in 10 ml CaCl₂ and kept at 4°C over night. The next day 2ml sterile 80% glycerol was added. 200 µl aliquots were frozen in liquid nitrogen and stored at -80°C.

Heat shock transformation of E.Coli:

100 µl competent E.coli Cells were mixed with 1 µg of plasmid DNA and incubated for 20 min on ice. Afterwards the cells were transferred into a 42°C heated water-bath for 2 min and for 10 min on ice. The cells were incubated with 0.8 ml LB medium at 37°C for one hour and plated on LB Agar (with 100 µg/ml ampicillin) and again incubated at 37°C over night.

Plasmid preparation (MIDI):

Cells from 50 or 100 ml o/n culture were harvested via centrifugation (5000 x g , 15 min at 4°C) Harvested cells were resuspended in 4ml Buffer S1+RNase (included in the Nucleobond–Kit) After resuspending, 4 ml of buffer S2 was added. The buffer S2 contains SDS and NaOH, because of these 2 ingredients the cells are lysed and the DNA is denatured. To neutralize the solution, 4 ml neutralization buffer (S3) was added. To separate the precipitated proteins and the chromosomal DNA, the solution was clarified via centrifugation (SS34; 15.000 rpm; 30 min; 4°C). The supernatant was applied to an equilibrated column (with 2.5 ml Equilibration Buffer). After one washing step (10 ml E3) the plasmid DNA was eluted with 5 ml elution buffer (E5). DNA in the eluted solution was precipitated with isopropanol and washed with 70% ethanol. The final DNA concentration was measured in the nano drop analyzer.

Restriction digest:

The total volume of one restriction digest was 50 μ l.

Contents:

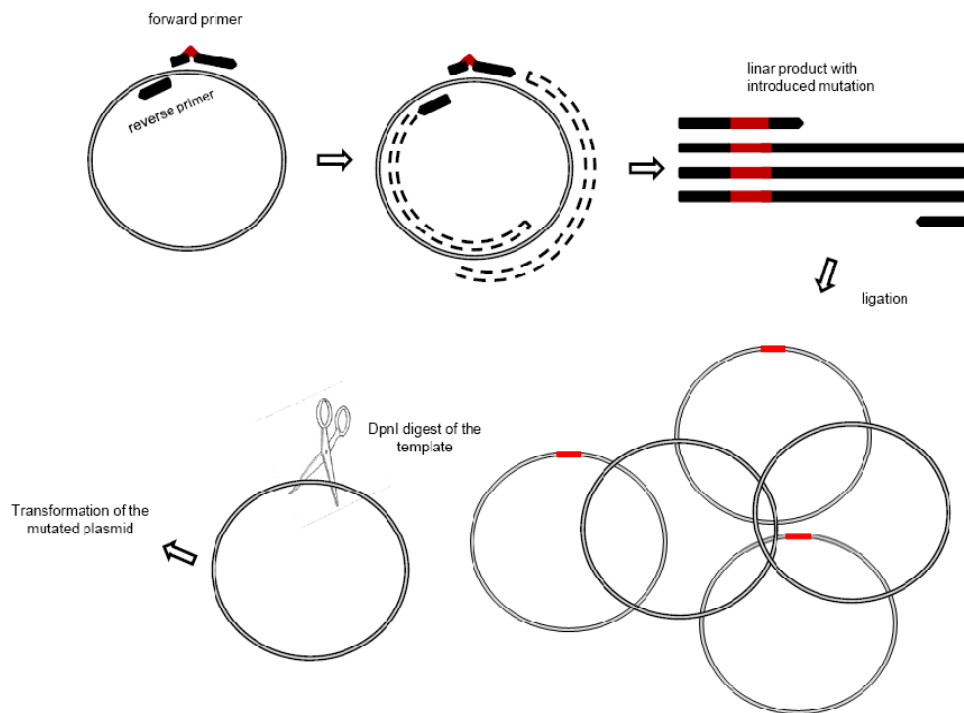
- 1 μ g plasmid DNA
- 5 μ l Buffer (NEB buffer 1 for AvrII/KpnI; NEB buffer 2 for Acc65I)
- 0.5 μ l BSA-solution (NEB) optional, only for special restriction enzymes
- x Water (autoclaved)

After mixing the solution was incubated for 2 hour at 37°C

10 μ l of the restricted volume were mixed with 2 μ l 6x loading Dye (Fermentas) and applied on a 1% agarose gel (total volume 40 ml). 0.5 TBE buffer was used as running buffer. DNA fragments were separated via electrophoresis with 80 V / 400mA for 50 min in a mini sub cell electrophoresis device (BIO-RAD).

Site directed mutagenesis (“round the horn”):

2 primers with different sizes were used for this method of site directed mutagenesis. Primer HRV2 loop1 was used as forward primer. This primer does not fully base-pair with the template sequence (indicated with red letters in the primer-list). The shorter reverse primer was complement to the template sequence. The amplification results in linear mutated strands that had to be ligated. To exclude that the template plasmid is transformed, it had to be removed before transformation. The template plasmid was amplified and isolated from an E.coli strain with active Dam methylase. This enzyme methylates the internal cytosine residues of DNA (plasmids). Because of this, it was possible to selectively digest the template DNA with the restriction enzyme DpnI, which only cleaves when its recognition site is methylated. After DpnI digestion the template sequence is fully digested and therefore not transformed in E.coli.



This site directed mutagenesis method comprises 3 different steps.

1. Phosphorylation of primers:

Primer stock solution should be 100 μM in water.

- 37 μl water
- 5 μl Kinase reaction buffer (NEB)
- 1 μl 50 mM MgSO_4
- 5 μl primer
- 1 μl 100 mM ATP
- 1 μl T4 PNK (NEB)

Incubation for 37°C for 60 minutes. Heat-inactivation at 65°C for 20 minutes.


2. PCR reaction:

The total volume of a PCR reaction was 50 µl

- 100ng template (HRV14-as3f WT)
- 5 µl 5x PFU polymerase buffer (Promega®)
- 125ng forward primer **HRV2_loop1**
- 125ng reverse primer **HRV14_3016rev.**
- 1 µl dNTP's (Promega® 200µM each)
- 1 µl Pfu Polymerase (Promega®)
- x water

PCR program:

1.	95°C	2 min	initial denaturation
2.	95°C	1 min	denaturation
3.	55°C	45 sec	primer annealing
4.	72°C	22 min	extension
5.	72°C	10 min	final extension
6.	4°C	∞	hold

 25 cycles

To verify whether the PCR reaction yielded the correct product, 10 µl of the PCR mix were applied on an agarose gel (1%). When the expected bands were observed, the remaining volume was digested (1h at 37°C) with 1µl of the methylation sensitive restriction enzyme DpnI.

3. Ligation of the PCR product:

- 2.3 µl water
 - 2.0 µl PCR product
 - 0.5 µl 10x T4 DNA ligase buffer (NEB)
 - 0.2 µl T4 DNA ligase
- incubation over night at RT

The entire volume of the mixture was used to transform competent E.coli (Top10) according to the heat shock transformation protocol; cells were plated out on LB agar plates supplemented with 100 µg/ml ampicillin (incubation o/n at 37°C).

Phenol-Chloroform extraction of DNA:

After the restriction digest with Acc65I (to obtain a linear plasmid) the mixture was filled up with 450 µl autoclaved water. 500 µl Phenol/Chloroform/Isoamylalcohol solution was added and mixed by vortexing. After centrifugation in an Eppendorf centrifuge (full speed; 2 min) the aqueous layer was transferred into a new tube. 50 µl 3M NaAc (5.2 pH) and 1 ml 100% ethanol was added. The mixture was vortexed and incubated for 20 min at -80°C. To pellet the precipitated DNA the sample was centrifuged (4°C, full speed).

DNA pellet was washed with 70% ethanol, dried and finally dissolved in RNase free water (50 µl).

***In-vitro* transcription:**

For the RNA transcription the Ambion® T7 MEGAscript kit was used.

The total volume was 20µl.

- 2 µl ATP
- 2 µl GTP
- 2 µl CTP
- 2 µl UTP
- 2 µl 10x reaction buffer
- 1 µg linear template (Acc65I cut and phenol/chloroform extracted HRV14_as3f WT)
- x Nuclease free water

After mixing, the solution was incubated at 37°C for 4 hours.

LiCl₂ precipitation of RNA:

The transcription reaction was stopped by adding 30 µl nuclease free water and 30 µl LiCl₂ solution. After mixing thoroughly the solution was chilled for 30 min at -20°C. To pellet the

RNA full speed centrifugation in an eppendorf centrifuge was carried out in the cold room (4°C). Subsequent a washing step with 70% ethanol the dried RNA pellet was dissolved in RNase free water. The RNA concentration was measured with the nano drop analyzer. RNA was stored at -80°C.

Preparation of HeLa cells for transfection and MaTra transfection:

Hela cells were seeded in a 6-well plate (cell count 0.375×10^6 per well in 3ml total volume in growth medium). When the cells had reached 80% of confluence they were washed with PBS and the medium was changed to infection medium (2ml). For the transfection 198µl Opti-MEM I medium was mixed with 1 µl RNA (conc. 3.0µg/µl) and 5 µl Matra reagent (IBA). For the control 200µl Opti-MEM I medium was mixed with 5µl Matra reagent (IBA). After vortexing, the mixture was incubated for 20 min at RT. The transfection-mixture was applied on the cells in the 6-well. For magnetic transfection a permanent magnetic plate was placed under the 6-well plate. The magnetic plate was removed after 15 min of incubation at 34°C. The cells were incubated for 2 days at 34°C.

Transfection of viral RNA with Lipofectamine2000:

80% confluent Hela cells were washed once with PBS and the medium was changed to infection medium (w/o antibiotics). 10 µl Lipofectamine2000 (Invitrogen) was mixed with 200 µl of MEM medium (w/o serum and antibiotics). The RNA (3 µg) was mixed with the 200 µl of serum free MEM. After 5 min of incubation at RT the RNA and the Lipofectamine2000 fraction were combined. Afterward an incubation time of 20 min the combined mixture (400 µl) was applied on the cells, which were incubated for 2 days at 34°C.

Preparation of [³⁵S]-radio labeled virus

First, a RNA transfection (Matra) of HeLa cells, using wt HRV14 and HRV14_HI2 RNA was carried out. The transfected cells were incubated for 3 days at 34°C. An aliquot of the supernatant (300 µl) from the transfected wells was used for infection of HeLa cells that were grown in a 6 well plate (80% confluent). The cells in the control wells were overlaid with virus at 10^8 TCID₅₀/well in 300µl infection medium (HRV2 and HRV14). After 1 hour of shaking at 34°C, 500ml methionine/cysteine free medium was added. To remove unbound virus the cells were washed with PBS after 3h of incubation. Then the cells were again incubated for 3 hour at 34 °C in 800ml methionine/cysteine -free medium. 0.1 mCi/well of [³⁵S]-methionine/cystein (Hartman Analytics Braunschweig, Germany) was added and cells were incubated at 34°C for 24 hours. The cells were broken by 3 freeze/thaw cycles and cell debris was removed by centrifuation in an Eppendorf centrifuge (14,000 rpm/10 min). The

supernatant was centrifuged in an ultracentrifuge at 70,000 rpm (rotor TLA 100.3, Beckman Instruments, USA) for 2 h at 4°C. The virus pellet was resuspended in 50 µl of virus buffer A. The resuspended virus was kept overnight at 4°C. The mixture was filled up with 1ml virus buffer A and re-centrifuged, to remove free unincorporated [³⁵S]-methionine/cysteine. The virus pellet was again resuspended in 50 µl of virus buffer A. Two µl of each sample were mixed with 5x reducing SDS sample buffer applied on a 15% SDS-PAGE. After running the gel, it was dried and exposed to Kodak BioMax MR film.

Preparation of Staphylococcus aureus cells

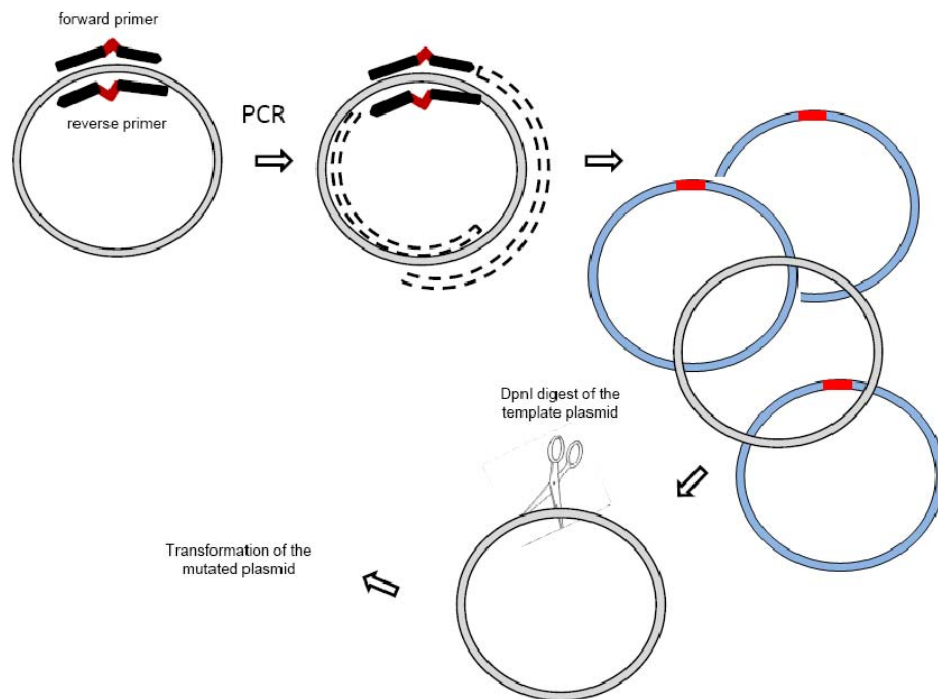
500 µl of a well resuspended Staphylococcus aureus (PANSORBIN) solution was pelleted via centrifugation and washed 2 times with PBS and once with RIPA buffer. After the last centrifugation the cells were resuspended in 400µl RIPA buffer and 100µl anti-HRV14 serum (rabbit). The cells were incubated at 4°C under continuous rolling over night.

Immune precipitation of the radiolabelled samples

Enrichment of radiolabelled virus particles was acquired by immune precipitation. 40 µl of the virus samples were mixed with 450 µl RIPA buffer and 25 µl of the Staphylococcus aureus cells with the bound anti HRV14 antibodies. After incubation for 1h under continuous rolling at RT the cells were centrifuged (4000 rpm, 10 min) and washed 3 times with RIPA buffer (500µl). The cells were resuspended in 40 µl RIPA buffer and 10µl 5x reducing SDS buffer were added. The samples were heated to 95°C for 5 minutes. This treatment is sufficient to reduce disulfides, solubilize and dissociate proteins without breaking the peptide bond. Finally 20 µl of the samples were applied on a 15% polyacrylamid gel and the gel was run. The gel was dried and exposed to Kodak BioMax MR film.

Site directed mutagenesis (quick change)

For the method of quick change site directed mutagenesis two primers with the same size were used. The mismatches are located in the middle of the primers flanked by 12 complementary nucleotides. No primer phosphorylation was needed, because the PCR ends in a circular product.



- 1 μ l plasmid template (45 μ g/ μ l)
- 10 μ l 5x Phusion® buffer
- 1 μ l dNTP
- 1 μ l primer **HRV14_K; HRV2loop1** (125ng/ μ l)
- 1 μ l primer **HRV14_Kcomp; HRV2loop1comp** (125ng/ μ l)
- 0,4 μ l Phusion® DNA Polymerase
- 35,6 μ l water

PCR reactions were performed in a Piko® Thermal Cycler (Finnzymes).

Program:

1.	98°C	3 min	initial denaturation
2.	98°C	5 sec	denaturation
3.	55°C	5 sec	primer annealing
4.	72°C	3 min	extension
5.	72°C	10 min	final extension
6.	8°C	∞	hold

 25 cycles

A subsequent DpnI digest was performed to get rid of the non mutated, methylated parental template DNA. 10 µl of the PCR mix were applied on an agarose gel. After having verified that the PCR yielded the expected bands, the mix was used to transform (heat shock transformation) competent E.coli.

Reverse transcription of Virus RNA

Exclude contamination with wt HRV14, the infective HRV14_HI clones were sequenced. HeLa cells were infected with HRV14_K and HRV14_HI2 viruses respectively and incubated for 2 days at 34°C 5% CO₂. The supernatant was 3 times freeze/thawed. Cell debris was removed by centrifugation in an eppendorf centrifuge (14,000 rpm, 10 min). The supernatant was centrifuged in an ultracentrifuge (70,000 rpm, 2h). The pellet was dissolved in Tris/HCl buffer (pH 8.5).

- 1 µl sample (in Tris buffer)
- 1 µl Primer (Primer 4)
- 1 µl dNTP's (Promega®)
- 1 µl RNAsin® (Promega®)
- 1 µl DTT (Invitrogen)
- 4 µl 5x Reverse transcription buffer
- 1 µl SuperScript® III reverse transcriptase (Invitrogen)
- 9 µl Nuclease free water (Promega®)

Program:

1.	55°C	10min	RNA release from eventually present virus
2.	4°C	3min	cooling step
3.	45°C	60min	reverse transcription
4.	70°C	15min	inactivate enzyme
5.	4°C	∞	hold


Amplification of the cDNA

To obtain double stranded DNA in sufficiently high amount for sequencing, a normal PCR reaction was performed.

- 1µl reverse transcribed DNA
- 1µl dNTP's (Promega®)
- 1µl forward primer 10pM (**HRV14_2420**)
- 1µl reverse primer 10pM (**Primer4**)
- 5µl 10x Pfu® buffer (Promega®)
- 0.4µl Pfu® DNA Polymerase (Promega®)
- 40.6µl water

Program:

1.	95°C	1 min	initial denaturation
2.	95°C	30 sec	denaturation
3.	50°C	30 sec	primer annealing
4.	72°C	90 sec	extension
5.	72°C	10min	final extension
6.	4°C	∞	hold

 25 cycles

After the PCR reaction 1 µl of the PCR mix was applied on an agarose gel (1%). An aliquot of the PCR mix together with the HRV14_2420 primer (10pM) were sent to the IMP sequencing service. The file containing the sequencing results was opened with CLC Sequence Viewer and aligned with the VP1 sequence of HRV14.

Virus infection assay

RD and RD-ICAM cells were grown in a 48 well plate to ~80% confluence. After washing with PBS, the cells were covered with 200 µl DMEM infection medium. Supernatant containing the chimeric HRV14 was added to the cells in 1:2 dilutions steps. The cells were incubated 3 days at 34°C 5% CO₂. The CPE was monitored by staining with crystal violet (1% in water).

Primer list:

>HRV2_loop1

CATTCAGAATAGTAA**CAGAGAAACACATT**CATAAAACTCTTGTC

>HRV2_loop1 comp

GACAAGAGTTTTATG**AATGTGTTTCTCTG**TTACTATTCTGAATG

44nt GC=31.8% TM=72.3°C *

>HRV14_3016rev.

CCATACTACCCATATGGTTTAGAA

24nt GC=37.5% TM=60.0°C *

>HRV14_2420

GTCCCCATACTAACTGCAAAC

21nt GC=47.6% TM=60.4°C *

>HRV14_K

CAGAATAGTAAATGAAAAGATGAACATAAAACTC

>HRV14_K_comp

GAGTTTTATGTTTCATCTTTTTCATTTACTATTCTG

35nt GC=25.7% TM=65.4°C *

>Primer 4

GGCTTTTCACAAATTATGGGGTAATAC

27nt GC=37.0% TM=65.9°C *

*calculated with the finnzymes TM calculator https://www.finnzymes.fi/tm_determination.html using the modified Breslauer's thermodynamics, dH° and dS° parameters [30]. Nucleotides that do not base pair correctly with the template sequence are in red.

Objectives:

Minor group human rhinoviruses use LDLR family members to attach to host cells. After the X-ray structure of HRV2 bound to a fragment of its cellular receptor was determined, new insights about the specific receptor recognition of a minor group virus were obtained by analyzing the structures. The receptor-recognizing part of the virion is VP1, more specifically the BC and the HI loop. The analysis of the structural data revealed that a strictly conserved lysine in the HI loop is the key player in the interaction of all 12 minor group viruses with these receptors. In the case of HRV2, lysine 224 in VP1 interacts with residues of the acidic cluster in the V3 repeat of VLDLR. The other important contribution of this lysine is a hydrophobic interaction with a tryptophan residue in V3. The lysine is conserved in all minor group viruses and obviously responsible for their receptor specificity. In 2006 all VP1 sequences of the known rhinovirus types were published; ten HRVs were found to also possess a lysine in the HI-loop at the equivalent position, however, these belong to the group of ICAM-1 binding rhinoviruses. Further investigations with respect to their LDLR binding abilities revealed that this group of major group viruses does not use LDL receptor family members for cell entry and hence are typical major group viruses. They were called "K-types". The VP1-VLDLR interaction cannot be uniquely determined by a single lysine residue in the HI loop of VP1. It is assumed that the interaction is born out of a combination of different interactions of amino acids, structural features of the surface loops, and the distribution of electrostatic charges on the surface of the interaction partners.

The aim of the presented work was to shed more light onto the basis of receptor recognition of minor group viruses. In particular, it should be attempted to change receptor specificity by a mutational approach and to classify minor group and K-type viruses by using bioinformatic methods.

3. Predictive bioinformatic identification of minor receptor group human rhinoviruses.

3.1 Introduction:

The goal of this project was to assess whether a simple and largely automated bioinformatic approach is able to classifying human rhinoviruses into the two receptor groups (major and minor group). Furthermore, we asked whether this approach can detect differences in binding of minor group and K-type viruses. In the following work we tried to obtain theoretical energy values that represent the binding affinity of rhinovirus protein VP1 to module 3 of the very-low density lipoprotein receptor (VLDLR).

3.2 Details of the rhinovirus - VLDL-receptor interaction:

Cryo-electron microscopy and X-ray structural analysis of complexes between HRV2 and recombinant receptor fragments [31,32] revealed that only VP1 interacts with the host receptor (VLDLR). Contacts between the viral protein and the receptor are located in loops that build a star-shaped dome at the five-fold axis close to the icosahedral vertex [33] . In picture 11 (left) the 3 VP1 surface loops of HRV2 are presented in ribbon representation. The picture on the right represents 2 symmetry related copies of VP1 interacting with V3 of VLDLR. The important amino acid residues of VP1 and V3 are labelled.

Because only VP1 is interacting with the VLDLR repeat 3 we only consider this protein for the following calculations. To mimic the structural interface of the virus–receptor binding, we use 2 copies of VP1 that are arranged in the same way as in the virion.

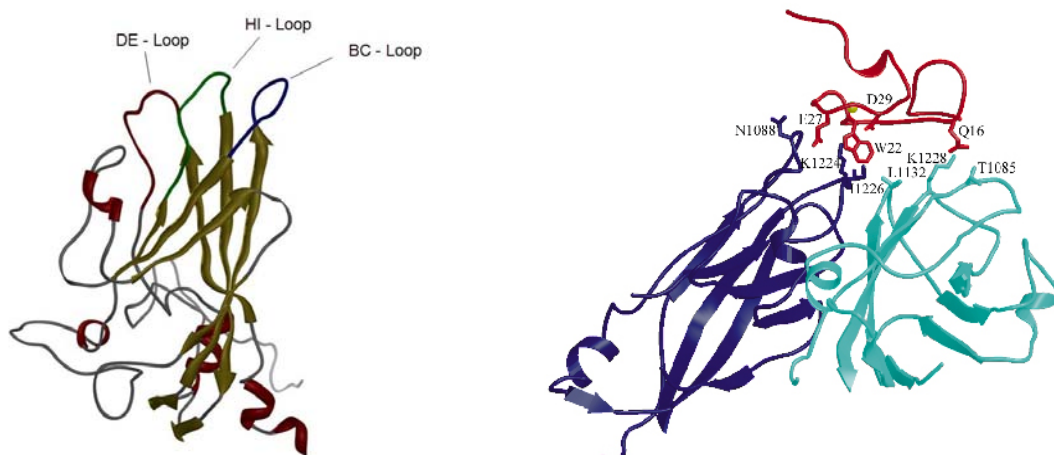


Figure 11: **left** 3D structure of VP1 with the receptor interacting loops. **right** 2 Two copies of HRV2 VP1 interacting with the module 3 of the very-low density lipoprotein receptor.

The key player in the interaction is a lysine at the position 224 in VP1 of HRV2. This lysine is strictly conserved within minor group viruses and it was believed that it was the only determinant for the interaction of minor group viruses and the LDL receptors. However, alignment of the VP1 sequences of all known HRV types revealed that some major group rhinoviruses also possess a lysine at the equivalent location. The types possessing a lysine residue in the HI loop are summarized in the alignment in figure 12. This lysine residue is found in 10 different HRV-types that were classified as non LDLR HRV's. These viruses cannot infect cell via LDLR and/or LRP; they are neutralized by soluble ICAM-1 [34], also the infection of HeLa cells can be blocked with a monoclonal antibody against ICAM-1 [35]. It was shown experimentally that some of these viruses are weak binders of MBP-V33333, whereas binding to LDLR was never observed. Because of the absence of binding, although possessing a lysine in the HI-loop, these rhinoviruses represent a quite interesting group within the rhinovirus genus. These viruses were consequently called “K-types”. Now the question arose, which additional interactions are responsible for binding of minor group viruses to VLDLR. However, there is no obvious conservation of any of the residues at the virus / receptor interface. Even when taking into account spatial vicinity within the three-dimensional structure, no obviously conserved amino acid pattern is apparent and only recently the basis of receptor specificity emerged as a combination of charge complementarity and hydrophobic interactions [36]. Hoping to obtain new insights about the specificity of binding of minor group and K-type viruses we started this project.

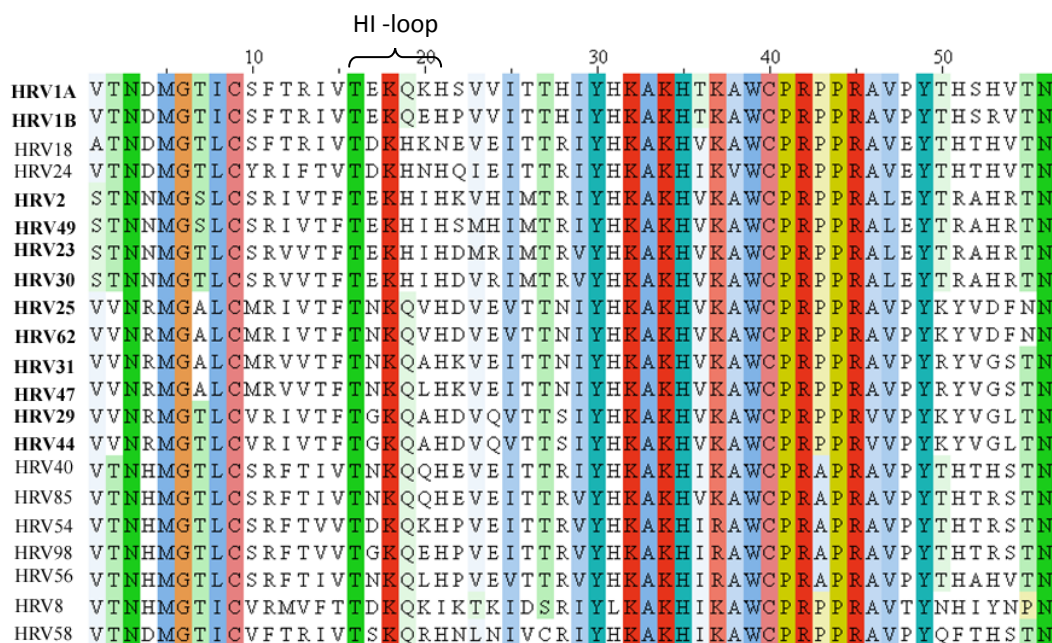
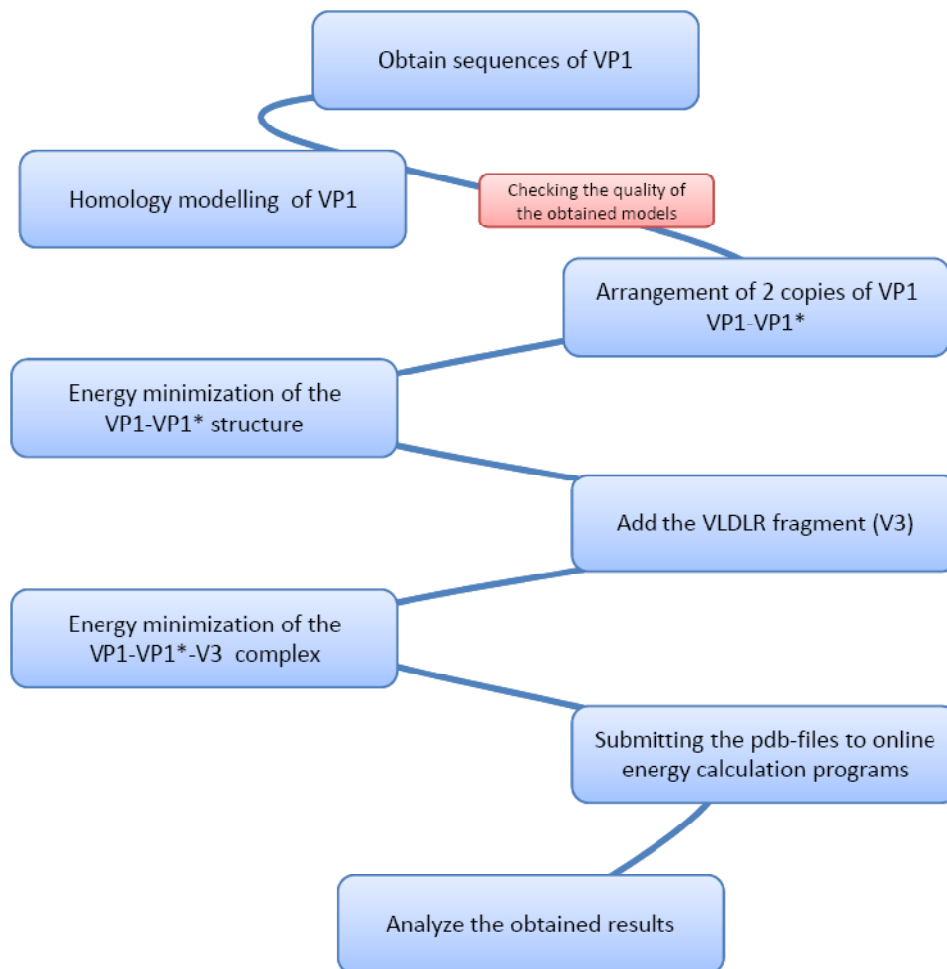


Figure 12: Alignment of minor group and K-Type viruses. The strictly conserved K in the HI loop is coloured in red. Virus types belonging to the minor group are written in bold.

3.3 Workflow of the method:



3.4 Modelling and evaluation of VP1 structures

The basis of our energy calculations are 3D structures of VP1. Unfortunately only a few X-ray structures of rhinoviral capsid proteins are determined. By now only X-ray structures of HRV1A, HRV2, HRV3, HRV14 and HRV16 are available. Since the number of possible folds in nature appears to be limited and the 3D structure of proteins is better conserved than their sequence [37], it should be possible to obtain 3D structures of VP1 for most of the 101 rhinovirus types. Moreover the characteristic folding of VP1, called beta-barrel jelly roll, which is a common folding of spherical viruses, is conserved in all rhinovirus types.

A homology modelling comprises usually four steps: (I) identification of structural templates (II) alignment of target sequence and template structures (III) model building and (IV) model

quality evaluation. The first three steps are carried out automatically by the Swiss-model workspace, which is a benchmark in homology modelling.

The VP1 sequences of the 101 HRVs [38] were downloaded from the UniProt knowledgebase. HRV87 has been identified to be an acid-sensitive enterovirus, EV68 [39], and was therefore not included. Note that based on antigenic cross reactivity and sequence similarity HRV8 and HRV95 were combined into one single type [38]. Since there are differences within the area equivalent to the receptor footprint they were considered as two separate types. The sequences were aligned with *ClustalW* and truncated by removal of 70 residues from the N-terminus and as many from the C-terminus as to leave 180 residues. The removal of the residues that are not in immediate proximity to the interface of VP1 and receptor should reduce the computer calculation time. The resulting sequences were submitted to SwissModel [40] in 'first approach mode' with default parameters by using a PERL script for automation. Except from HRV7 and HRV69 models were obtained for all HRVs. For the latter two, no structure was obtained by Swiss-model using the first approach mode. The 2 types were excluded from the analysis, being aware that the optimized mode of swiss-model [41], can obtain a structure, when the 3D structure of HRV3 was used as a template. To avoid too much bias we decided to simply exclude these two types from the subsequent analysis. Finally, 3D models of 99 VP1 proteins including the BC, DE, and HI loops making up the receptor-binding epitope were obtained.

3.5 Evaluating the result of the homology modelled VP1 structures:

Assessing the quality of the obtained 3D VP1 models, we used the following approach. The 5 VP1 sequences of rhinoviruses, whose experimental structures are available, were modelled using the project mode of the swiss-model webpage, selecting the second best template for modelling. In this way we excluded that swiss-model considers the experimentally determined 3D structures from modelling. The table 4 shows the obtained RSMD values for the modelled VP1 structures. All models were within less than 0.65 Å RSMD for the backbone and less than 0.74 Å with the side chains included, from the experimental structure indicating good quality of the models.

To retrace which templates were selected by 'automatic mode' of SwissModel to model the different structures of the HRV types we summarized the usage of templates in Fig. 5. In accordance with the phylogenetic relationships [42] the program automatically selected the PDB coordinates of B-type viruses HRV3 and HRV14 as templates for modelling of VP1 of the other B-types. For modelling the A-type viruses, coordinates of HRV1A, HRV2 or

HRV16 were automatically chosen as templates for modelling. With regard of the receptor groups there was no particular preference of the minor group types for any of the type-A templates whereas for the K-types only HRV1A was used. As expected, for those types whose experimental structure was available (HRV1A, 2, 3, 14, and 16) their corresponding data were selected for model building. It turned out that some types were more often used as templates than others. Surprisingly HRV1A seems to be the most universal template as it was used for more than 50 % of all HRVs.

Type	used template	RMSD C α	RMSD backbone + side chains
HRV1A	1aym [HRV16]	0,64 Å	0,73 Å
HRV2	1aym [HRV16]	0,57 Å	0,60 Å
HRV3	1k5m [HRV14]	0,50 Å	0,53 Å
HRV14	1rhi [HRV3]	0,50 Å	0,55 Å
HRV16	1r1a [HRV1A]	0,61 Å	0,70 Å

Table 4: Quality of the 3-D modeling. Models of HRVs whose 3D structure is known were automatically built by excluding themselves as template. Sequences were submitted to "template search" in SwissModel and the "second best template" (parenthesis) was chosen for modeling with "optimized project mode". RMSD (root mean square deviation) was derived from superposition of models and experimental structures by using the "iterative magic fit" function in SPDBV4.0.

HRV1A				HRV 2	HRV 3	HRV14	HRV16
<i>lr1a</i>				<i>lfpn</i>	<i>lrhi</i>	<i>lk5m</i>	<i>laym</i>
1A	95	39	65	2	70	5	25
1B	98	41	66	23	91	6	62
29	11	43	68	30	3	14	10
31	12	46	71	49	4	27	16
44	13	50	73	9	17	37	21
47	15	51	74	32	26	48 *	45
8	19	53	75	67	35	52	77
18	20	55	76		42	72 *	81
24	22	57	78		79	84	90
40	28	59	80		83	86	96
54	33	60	82		92	93	100
56	34	61	88		99	97	HANKS
58	36	63	89		*1rud		
85	38	64	94				

Table 5: Templates automatically selected by SwissModel for modeling VP1 of all HRVs. Blue, minor group; red, genus A major group; green, K-types; orange, genus B major group; grey, HRV70 and HRV91 whose modeling led to strong crashes with V3. Striped, HRVs whose 3D X-ray structures are available. Note that in case of HRV48 and HRV72 the structure of HRV14 containing the antiviral capsid-binding hydrophobic antiviral compound WIN 52084 [43] was automatically selected for modeling (accession number 1rud).

3.6 Modelling VP1-VP1*-V3

Since the footprint of V3 extends over two symmetry-related copies of VP1, VP1-VP1* 'dimer' were assembled by superposition onto the experimental structure of VP1-VP1* of HRV2 by 'magic fit' using an SDBV4.0 script [44]. The correct coordinates for the dimerization were taken from the oligomer generator at the viper-db site [45]. The VP1-dimers were minimized with the Gromos96 [46] force field energy minimization method (100 cycles, steepest decent, which is part of SPDBV). The assembly of the 2 copies of VP1, as well as the energy minimization was carried out with SPDBV 3.7 with a script. The final structures of the respective VP1-VP1*-V3 'trimers' were obtained by superposition and combination with the coordinates of V3 taken from the HRV2-V23 X-ray structure [33]. The Ca²⁺ ion that is complexed by the receptor is not considered because no topology was available in SPDBV. Coordinates of these complexes were again energy minimized as above.

During the assembly of 2 VP1 models with V3, chain identifiers were allocated to the different peptide chains. The two VP1 chains received the chain IDs 'A' and 'B'; the receptor received the chain ID 'R'. The chain IDs are important for the submission to energy calculation servers. These 'trimers' (VP1-VP1*-V3) were again minimized as above. Modelling of the HRV70 and HRV91 receptor complexes did not result in reasonable structures as their BC loops clashed with V3; this problem was not resolved by energy minimization (See structures in Fig. 13). As HRV70 and HRV91 are typical major group HRVs and not K-types we made no further effort to improve the models and excluded them from further analysis.

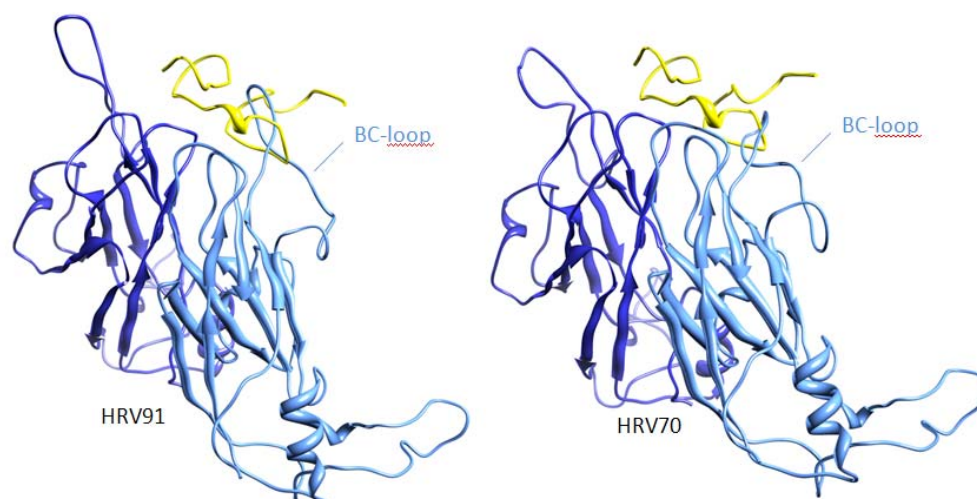


Figure 13: Steric clashes of the BC-loops of HRV91 (left) and HRV70 (right) and the receptor. VP1 and VP1' colored in blue. VLDLR repeat 3 colored in yellow.

3.7 Energy calculations

Models of VP1-VP1*-V3 were submitted to the Dcomplex web server [47] (<http://sparks.informatics.iupui.edu/song/complex.html>); datasets were entered and results retrieved automatically by using a PERL script. One set of data containing VP1-VP1*-V3 coordinates that had been energy minimized in *SPDBV3.7* (as described above), the other contains files that were energy minimized with *Jackal minst* (30 cycles).

Models were also submitted to the *FastContact2.0* web server (<http://structure.pitt.edu/servers/fastcontact/>). Three different data sets were submitted to the fastcontact webservice. Similar to the 2 different datasets that were submitted to *Dcomplex*, these datasets only differed in the way their energy was minimized. One set was again prior energy minimized by *SPDBV 3.7* the other by *Jackal*. (100 cycles for *SPDBV*; 30 cycles for *Jackal*). The used number of cycles in the jackal and SPDBV minimization was chosen after different test runs, where the same protein was minimized with different number of cycles, followed by comparison of the energy values. Higher values than those we have used (30 cycles in *Jackal*; 100 cycles in *SPDBV*), only marginally lowered the energy of the protein, therefore we did not use a higher number of cycles. The third set of data contained the coordinates without any prior energy minimization. With this set of data we wanted to show whether prior minimization is required to obtain good a classification of the respective HRVs. Note that the online version of *Fastcontact 2.0* performs an energy minimization using *CHARMm* parameters.

Before the VP1-VP1*-V3 structures can be submitted to the *Fastcontact 2.0* web server, they have to be dissected into 2 files; one containing the receptor (V3), the other one containing the VP1 'dimer'. This separation of the files was carried out by using a script. The submission to *Fastcontact 2.0* was done manually. A local copy of the *Fastcontact* program, kindly provided by the author [48,49], that is not able to minimize the entered structures with *CHARMm*, was tested as well.

3.8 Result of the energy calculations

Having verified that our approach resulted in 3D models very well matching the known X-ray structures, we assumed that the other models were plausible and close to reality. Thus, we next asked whether the binding energies calculated for the complexes between the receptor module and the respective virus correlate with the classification established from binding experiments [35,50]. All models were either energy minimized with the *SPDBV*-inbuilt *GROMOS96* or with *Jackal* [51] (<http://trantor.bioc.columbia.edu/programs/jackal>) and subjected to energy calculation via *Fastcontact 2.0* and *Dcomplex*. As the *Fastcontact* online server again energy minimize the structures using the program *CHARMm*, in order to prevent automatic minimization with *CHARMm*, therefore we tested a that does not include the minimization step, a local copy of *Fastcontact 1.0* was tested as well. In this case the coordinates were only minimized with the *SPDBV* inbuilt *Gromos96*. The results of the calculations are summarized in Figures 14 and 15. Overall, major and minor group viruses were quite well separated by *Fastcontact* regardless of the minimization method used (Fig. 14 A-C). When taking the correct classification of minor group HRVs as a criterion, *Fastcontact 2.0* run on the webserver clearly gave the best results (Fig. 14 A). Nevertheless, drawing a threshold line either included 2 K-type viruses (HRV18, 98) in the minor group or led to misclassification of two minor group viruses (HRV2 and HRV47) that were then grouped together with the K-types. The separation of minor group HRVs and K-types was heavily compromised when minimization by *SPDBV* was omitted and carried out by the web based *Fastcontact* alone (Fig. 14 B). Minimization with *Jackal* did not improve this situation (Fig. 14 C) and *Dcomplex* was even unable to reliably separate the minor and the major group, neither after minimization with *SPDBV* (Fig. 15 D) nor with *Jackal* (Fig. 15 E). Results obtained from the local copy of *Fastcontact 1.0* where not reasonable suggesting that the additional *CHARMm* minimization step, that is not included in the local executable program of *fastcontact* is important to obtain reasonable results. (data not shown). It is also possible that this earlier version of *fastcontact* has inferior performance.

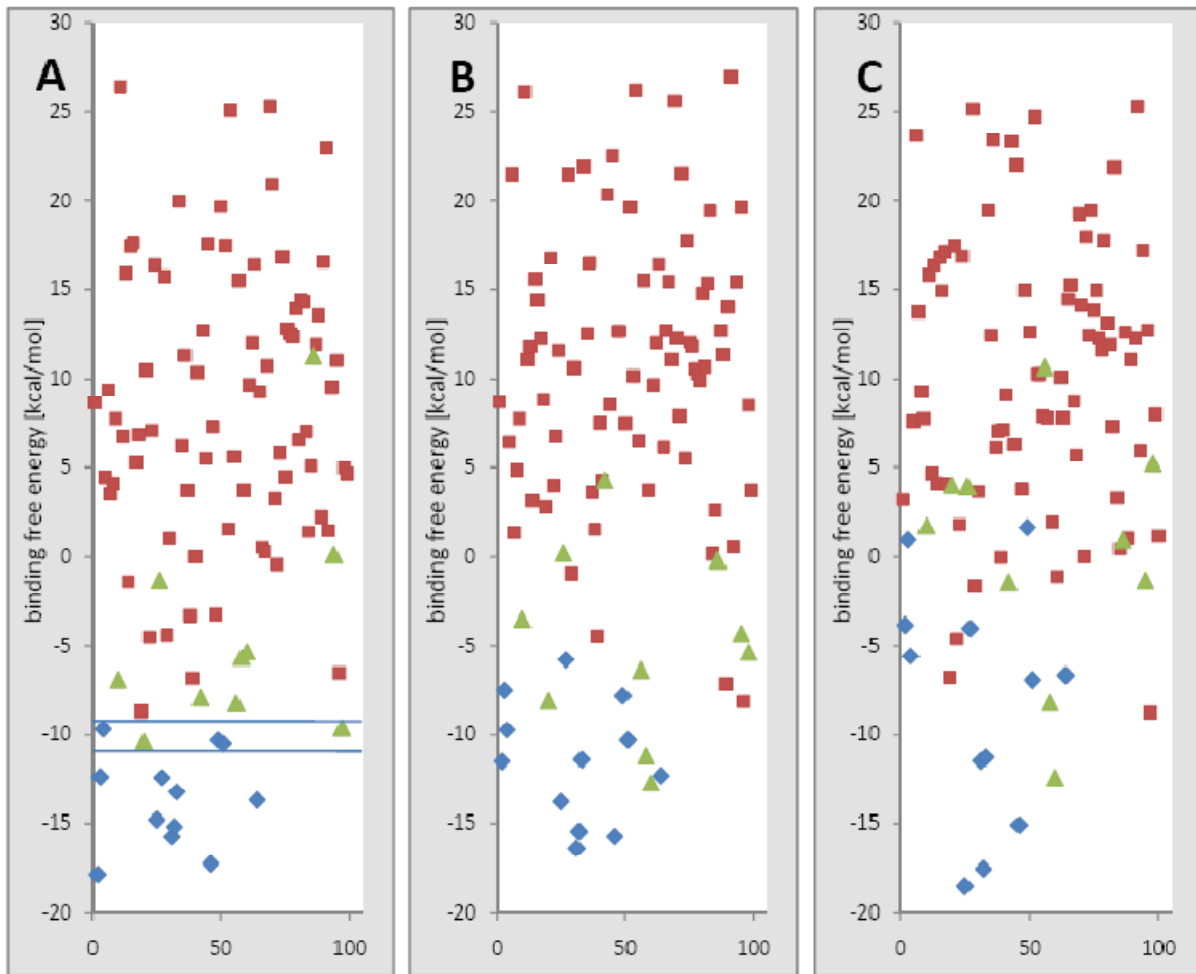


Figure 14. Net interaction free energy (sum of the desolvation and the electrostatic energy) of the binding of V3 to 97 HRV types, listed on the horizontal axis, calculated with A) FastContact webserver after energy minimization with *SPDBV3.7*, B) FastContact webserver without prior energy minimization with *SPDBV3.7*, C) FastContact webserver after energy minimization with Jackal. The viruses are positioned according to their number. Minor group viruses are colored in blue, major group viruses in red and K-type viruses in green.

The best method of energy calculation (*Fascontact 2.0* online server; Fig. 14A) could separate all non-K-type major group viruses from the minor group viruses. However, the K-types HRV18 and 98 and the minor group viruses HRV2, HRV47, and HRV49 (between the two lines) exhibit almost the same predicted binding affinities.

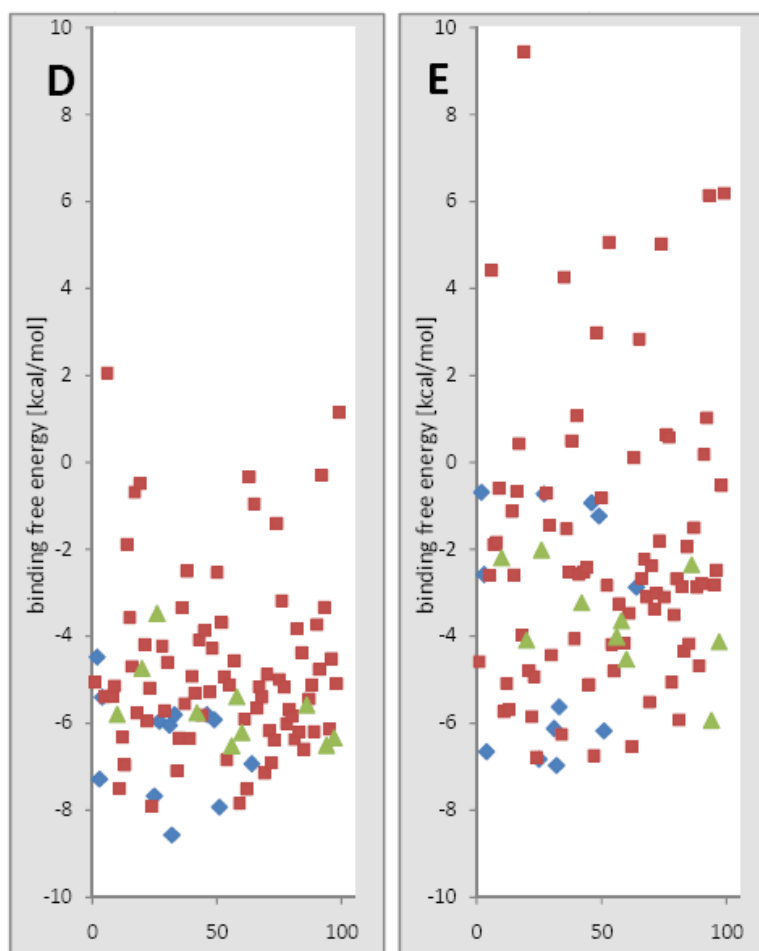


Figure 15: Results of the free energy calculation with Dcomplex either energy minimized with SpdbV3.7 21D or with Jackal seen in 21E. In both cases it was not possible to distinguish between major and minor group viruses. Major (red), minor (blue), and K-type viruses (green) are positioned according to their number.

3.9 Correction of calculated affinities:

Fastcontact not only calculates the electrostatic (4r), desolvation free, and the van der Waals (CHARMm19) energy but also outputs the twenty residue pairs with lowest (attraction) and highest energy values (repulsion), respectively. A closer inspection of the 10 best and 10 worst energy contributions of receptor-VP1 interaction, drew our attention to the first cysteine in the receptor module that forms a disulphide bridge with the 3rd cysteine [52] because it unexpectedly was in the list of interacting residues. Fastcontact also sends back the coordinates corresponding to the energy-minimized structure used for calculation of the binding energies; this enabled us to visually inspect these coordinates. It revealed that all disulphide bridges had been opened thereby providing -SH groups potentially interacting with residues of the virus (see Fig. 16).

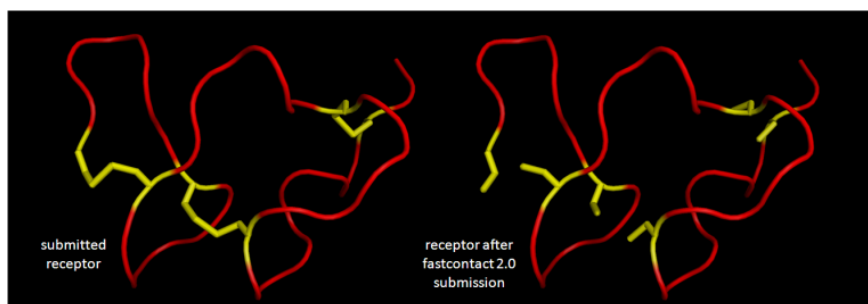


Figure 16: A ribbon presentation of the VLDL receptor module 3 before (left) and after fastcontact submission (right).

Presumably the free $-SH$ groups of the cysteines were able to establish hydrogen bonds to suitable oxygen atoms nearby which were taken into account in the energy calculations. For the reasons mentioned above, these cysteine interactions are not meaningful and can be definitely excluded. Therefore, we subtracted the energy values contributed by the receptor cysteines from the total sum of the interaction energies. This strongly improved the final result. The representation of the corrected binding affinities can be seen in Figure 17. It was now possible to draw a line that separates all minor group viruses from the K-type viruses. The highest binding affinity was calculated for HRV8 that is known to exhibit weak binding to the pentameric fusion protein MBP-V33333.

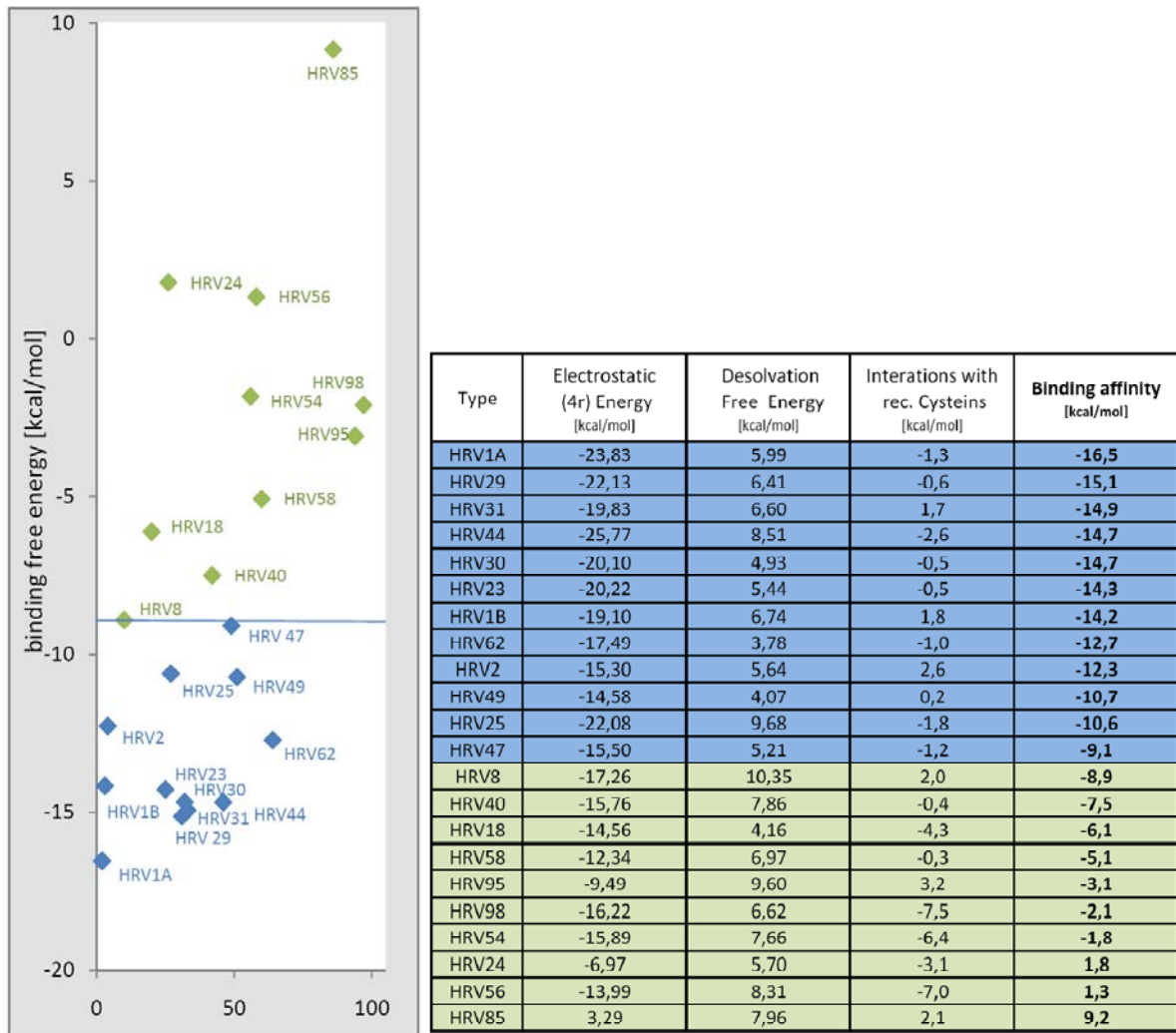


Figure 17: Energy table of all minor group and K-Type viruses and representation of the final results. Minor (blue) and K-Type (green) viruses are perfectly separated (separation line). Note that the not meaningful cystein interactions are subtracted from the predicted energy values.

3.10 Evaluation of the results:

Minor group viruses and K-types were successfully separated. However the differences between HRV47 and HRV8 were marginal. Neutralization experiments with VLDL-receptor derivatives did show a strong neutralization in the case of HRV47, whereas infection of HRV8 could not be blocked [33,50]. Neutralization assays are not the best way to demonstrate VLDLR-binding of minor group viruses, because major group viruses, like HRV8 use ICAM-1 for cell entry. A better assay for demonstrating binding of K-type viruses is a virus overlay blot. Since interaction of single receptor modules is very weak (even with minor group HRVs) and only increases upon concatenation [53,54], maltose binding protein fused to five consecutive copies of V3 (MBP-V33333) was used for binding experiments [55]. The data presented in Fig. 18 was obtained by Khan, A.G. It shows that the in-silico binding results match the experimental observations. This figure shows the result of a ligand

binding blot using HRV2, HRV8, HRV85 and HRV14. As expected from my calculations, HRV8 indeed bound this receptor derivative weakly when compared to HRV2 that exhibited very strong binding. The K-type virus with the lowest predicted affinity, HRV85 showed no detectable affinity for the VLDLR-concatemer MBP-V33333. No binding was seen in case of HRV14. This further demonstrates that an approximate prediction of the relative affinities from 3D models is possible although the absolute values are certainly not correct.

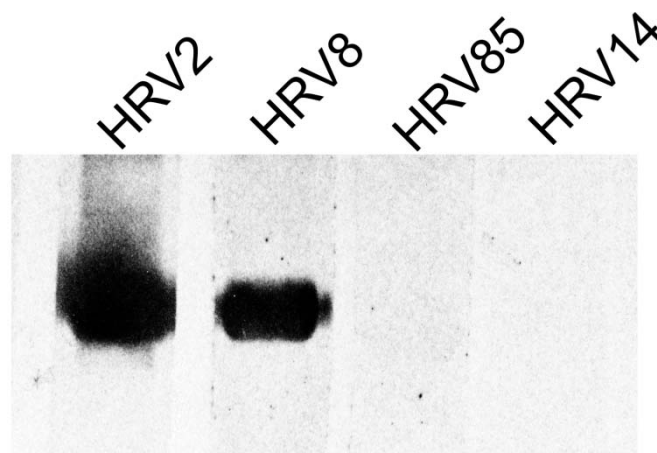


Figure 18: Ligand blot to detect binding of radiolabeled HRVs to MBP-V33333. Recombinant receptor was run on an SDS 10% polyacrylamide gel under non-reducing conditions and transferred to a PDV-membrane. Strips were incubated with 20,000 cpm each of ³⁵S-methionine labeled virus as indicated and exposed to X-ray film. Note binding of HRV2, weak binding of HRV8 and absence of binding of HRV85 and HRV14.

3.11 Different contribution of amino acid residues to the binding energy:

According to the affinities minor and K-types are well separated. The question arose whether minor group and K-type viruses show different binding patterns. The 10 best and the 10 worst interactions, taken from the text-file that is part of the *Fastcontact* output, are represented in a heat map. The energy values of the interactions of receptor (V3) and VP1-VP1* dimer are indicated in the boxes in kcal/mol. Negative energy values are colored in different shades of red. Repulsive interactions with positive energy values are presented in different shades of blue.

As expected, even in the K-type viruses, that show very weakly binding to the receptor, the lysine in the HI loop clearly emerged as the central player by interacting with glutamic and aspartic acid residues in the acidic cluster around the central Ca²⁺ ion of the receptor module.

In addition, various other residues were seen to differently contribute. The low binding affinity of HRV85, that showed undetectable binding affinity in the ligand blots, can be explained with a high repulsive interaction of D89 in the first copy of VP1 and E25 in the receptor.

HRV1A	E 5	T 13	Q 14	V 18	S 19	W 20	D 23	E 25	D 27	E 34
D 88							1,3	1,4		
K 157								-1,1		
E 227								0,5	0,9	
K 224					0,4	1,4	-6,2	-5,4	-1,5	-0,8
K 230				0,6						
K 83									-4,2	
D 85			1,8						1,0	
Y 86		-0,8								
R 134									-2,9	
K 230	-0,8									

HRV47	I 6	T 13	Q 14	P 17	W 20	D 23	E 25	D 27	D 33	E 34
E 155							-0,7			
H 156							1,0			
K 224						1,5	-6,0	-4,9	-1,6	-0,5
N 85			1,1							
E 86	0,7		0,6							
Q 87			0,6							
Y 130				-0,5	-0,7				0,5	
K 228	0,8									
E 230									1,2	

HRV29	Q 14	I 16		W 20	D 23	G 24	E 25	D 27	E 34
D 89					0,3		0,6		
K 91							-1,3		
R 154							-0,7		
K 224				1,3	-5,9		-4,2		-0,8
D 228					0,3		0,3		
K 83								-0,7	
Q 86	0,6								
R 130		0,7						-1,2	
K 224									
D 228	0,3								

HRV8	E 5	I 6		Q 14	W 20	D 23	E 25	D 27		E 34
D 87						1,3	2,3			
K 154							-1,2			
R 155							-0,6			
K 225					1,3	-6,4	-4,8	-1,6		-0,8
K 227	-0,6									
E 83								1,1		
D 85				1,2						
K 132	-1,2	1,6								
K 227	-0,9									
K 229		0,7								
K 231									-1,4	

HRV31		I 6		S 19	W 20	D 23	E 25	D 27	D 33	E 34
D 85						0,3	0,3			
D 89						0,4	0,6			
K 91							-1,7			
R 154							-0,7			
K 155							-0,5			
K 224				-0,5	0,9	-6,7	-3,7	-1,6	-0,5	-0,9
K 224										
K 228		0,8								
E 230						0,5	1,1			

HRV40	E 5	Q 14	I 16	S 19	W 20	D 23	E 25	D 27		E 34
S 87				-1,2			0,7			
L 88							0,7			
D 91							2,5			
R 157							-0,7			
K 227					1,6	-8,4	-5,3	-1,5		-0,8
D 85			0,6					1,8		
N 86		0,8								
E 89		-1,5								
K 133								-0,9		
E 135	0,6									
E 231										
E 233								1,3		

HRV44	T 13	Q 14	I 16		S 19	W 20	D 23	E 25	D 27	E 34
N 89								1,4		
D 163								0,6		
R 154								-0,7		
K 224					0,4	1,4	-5,7	-4,9	-1,5	-0,8
K 83			0,4						-4,9	
N 85		0,9								
Q 86	0,4	0,8								
R 130			0,6						-1,3	
K 224										
D 228										

HRV18	E 5		W 20	C 22	D 23	E 25	D 27		E 34
E 87			0,7		2,4				0,9
D 88					0,8	0,8			
N 90						0,9			
D 159						0,7			
K 228			1,5		-7,1	-5,3	-1,5		-0,8
K 81							-0,9		
Y 86									
E 87									
K 134							-0,9		
K 230	-0,8								
E 234							1,2		

HRV30						W 20	D 23	E 25	D 27	E 34
E 85							0,5	0,9		
L 86								1,2		
A 87							1,1	0,8		
Y 89								-1,0		
D 90								1,1		
R 156								-0,9		
E 223								0,5		
K 224						1,7	-3,8	-5,3	-4,0	-0,8
K 81									-1,8	
E 83									1,1	
L 132						-0,7				
D 228										
R 230						0,4			-3,6	

HRV58	E 5	Q 14	P 17	V 18	S 19	W 20	D 23	E 25	D 27	E 34
K 86							-0,9	-1,5		
T 87					-0,5		0,7			
D 90								2,4		
D 91								1,0		
R 158									-0,6	
K 228						1,0	1,6	-4,7	-2,2	-1,5
R 230	-0,6		1,1	0,7						
K 81										-0,9
N 85		0,7								
E 86		0,9								
E 136	0,6									

HRV23						W 20	D 23	E 25	D 27	E 34
E 85							0,5	0,9		
I 86								1,0		
G 87							1,1	1,3		
N 88								0,5		
D 90								1,4		
E 91								0,6		
R 156								-0,9		
K 224						1,6	-3,5	-6,1	-3,9	-0,8
K 81									-1,2	-1,5
K 83										
L 132						-0,7				
D 228										
R 230						0,6			-2,7	

HRV95			P 17	V 18	W 20	D 23	E 25	D 27		E 34
H 86							1,5			
D 87						5,0	2,1			1,2
D 90							1,4			
R 155							-0,7			
K 225					1,2	-3,2	-10,0	-3,4		-0,6
K 227		1,6	1,5							
E 83								0,9		
D 87										
I 131		-0,6		-0,7						
K 229										
K 231							-0,6	-1,9		

HRV18	R 2	E 5	I 6	Q 14	S 19	W 20	D 23	E 25	D 27	E 34
D 85							1,2	1,8		
N 87								-1,5		
E 227									0,8	
K 228					0,6	1,6	-4,0	-4,5	-1,9	-0,8
E 230	0,8									
K 83									-3,2	
D 85									0,8	
Y 86			-0,9							
D 88				0,7						
K 94				2,3						
R 134									-1,8	
C 250	-1,3									

HRV98	E 5	Q 14	S 19	W 20	D 23	E 25	D 27	D 33	E 34
D 87			0,8		2,4	0,9			
V 88						1,1			
E 89					1,3				
N 91						1,2			
K 156						-1,2			
R 157						-0,7			
K 227				1,5	-7,1	-5,3	-1,4	-0,5	-0,8
E 229	0,9								
D 87		0,8							
K 133							-1,0		
E 233							1,3		

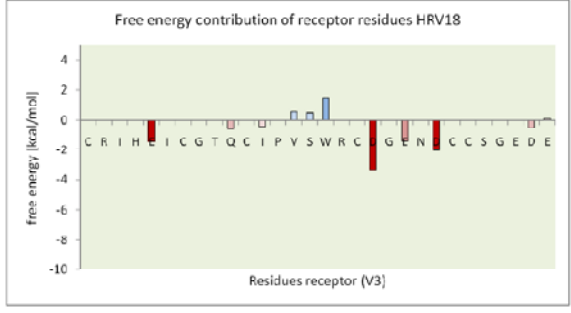
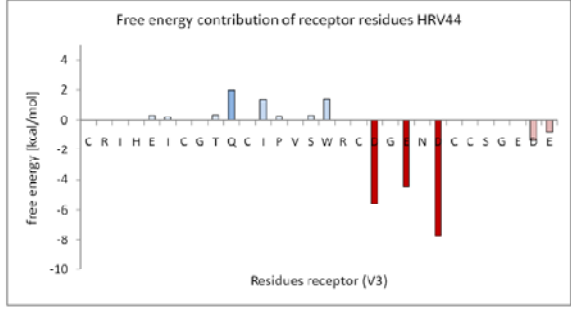
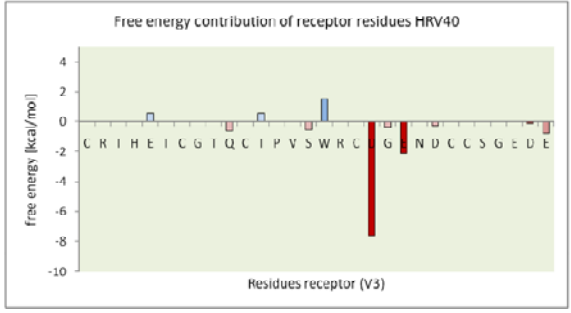
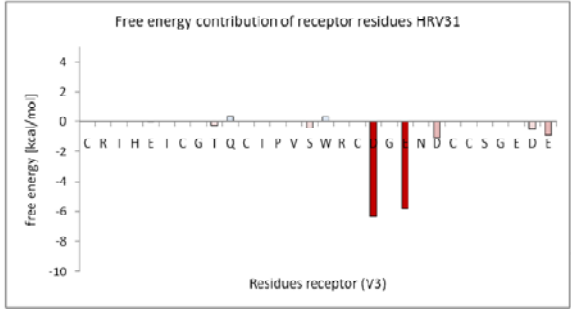
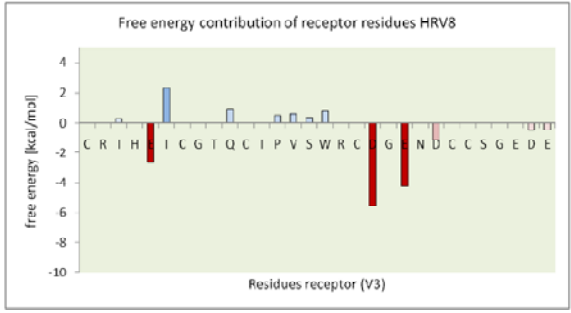
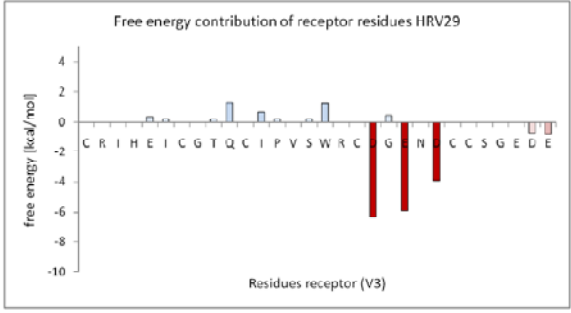
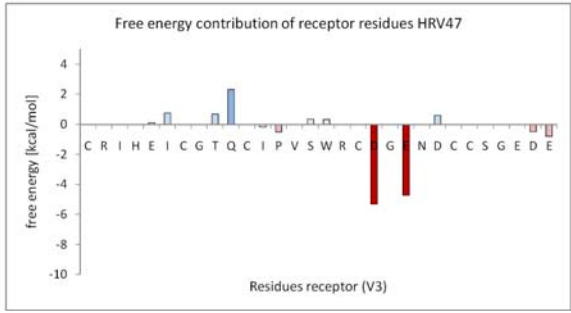
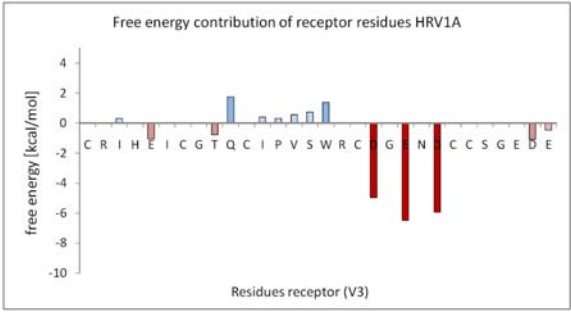
HRV62		Q 14	I 16	S 19	W 20	D 23	E 25	D 27		E 34
K 89							-1,6			
D 90						0,4	0,5			
D 153							0,6			
R 154							-0,7			
K 224				0,4	1,3	-5,5	-4,8	-1,6		-0,8
E 83								1,9		
L 86		-1,5								
R 130			0,6					-1,2		
K 224										
D 228										
E 230						0,5	1,1			

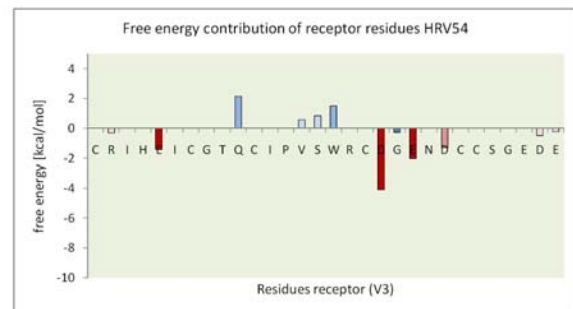
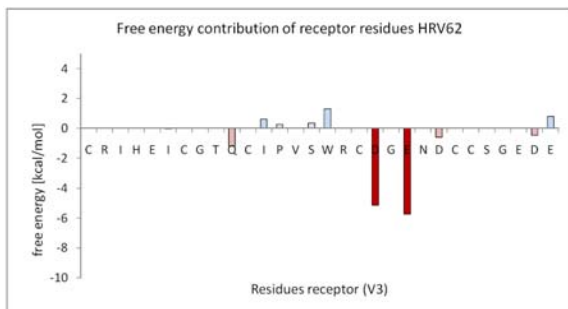
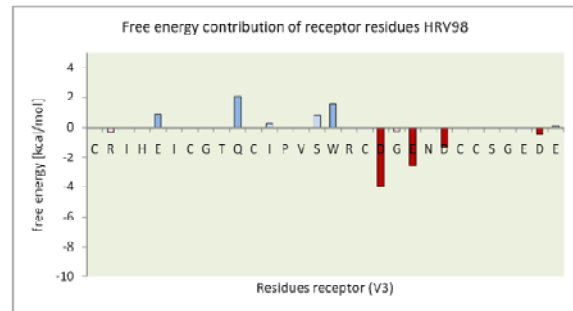
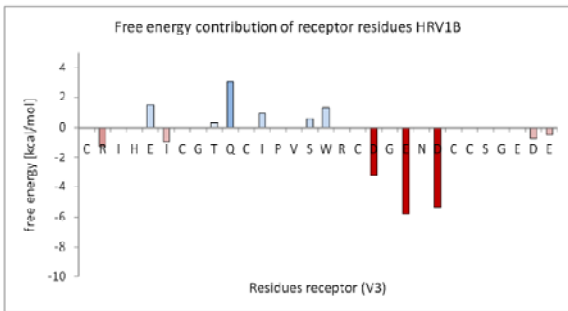
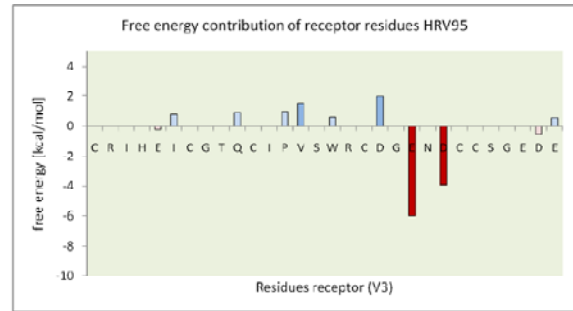
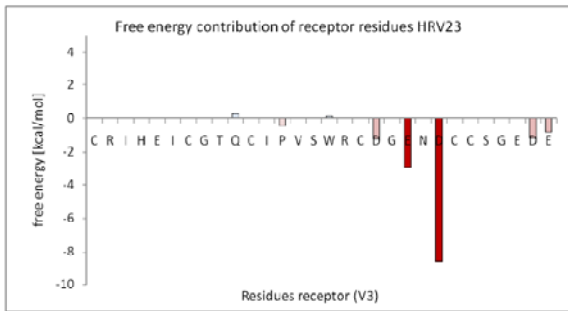
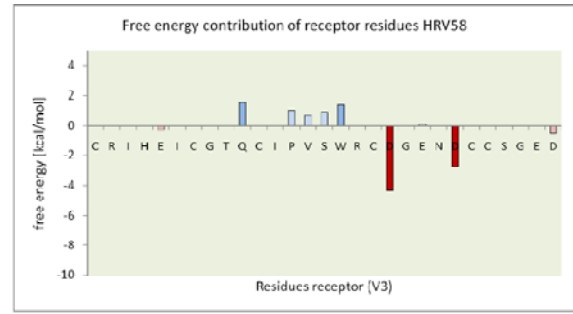
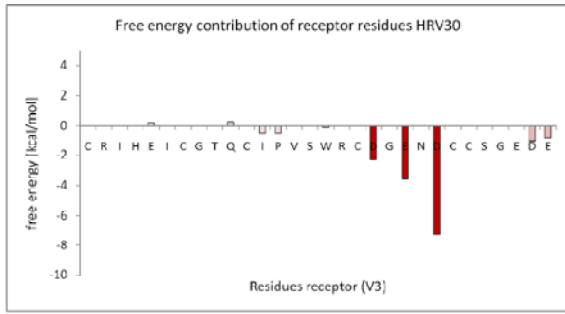
HRV54	E 5	Q 14	S 19	W 20	D 23	E 25	D 27		E 34
D 87			0,8		2,4	0,9			
V 88						1,1			
E 89					1,0	0,7			
N 91						1,2			
K 156						-1,2			
R 157						-0,7			
K 227				1,5	-6,8	-5,5	-1,5		-0,8
K 229	-0,6								
D 87		0,8							
K 133							-1,0		
K 229	-0,8								
E 233							1,3		



Figure 19: Heatmap representation of the 10 best (attraction) and 10 worst (repulsion) interactions of the VP1-VP1*-V3 complex. The interacting residues of the receptor are presented horizontally. Vertically presented are the interactions with the 2 copies of VP1. Residues of the first copy are in **bold**; residues of the second copy are in *italics*. Energy values are given in kcal/mol.

To check whether there are significant differences in the interaction of minor group and K-type viruses with respect to receptor interactions, bar diagrams depicting the contribution of each of the receptor residues were drawn for all minor and K-type viruses. (Fig. 20) The sum of the interaction energies of the single receptor residues were represented in vertical bars.





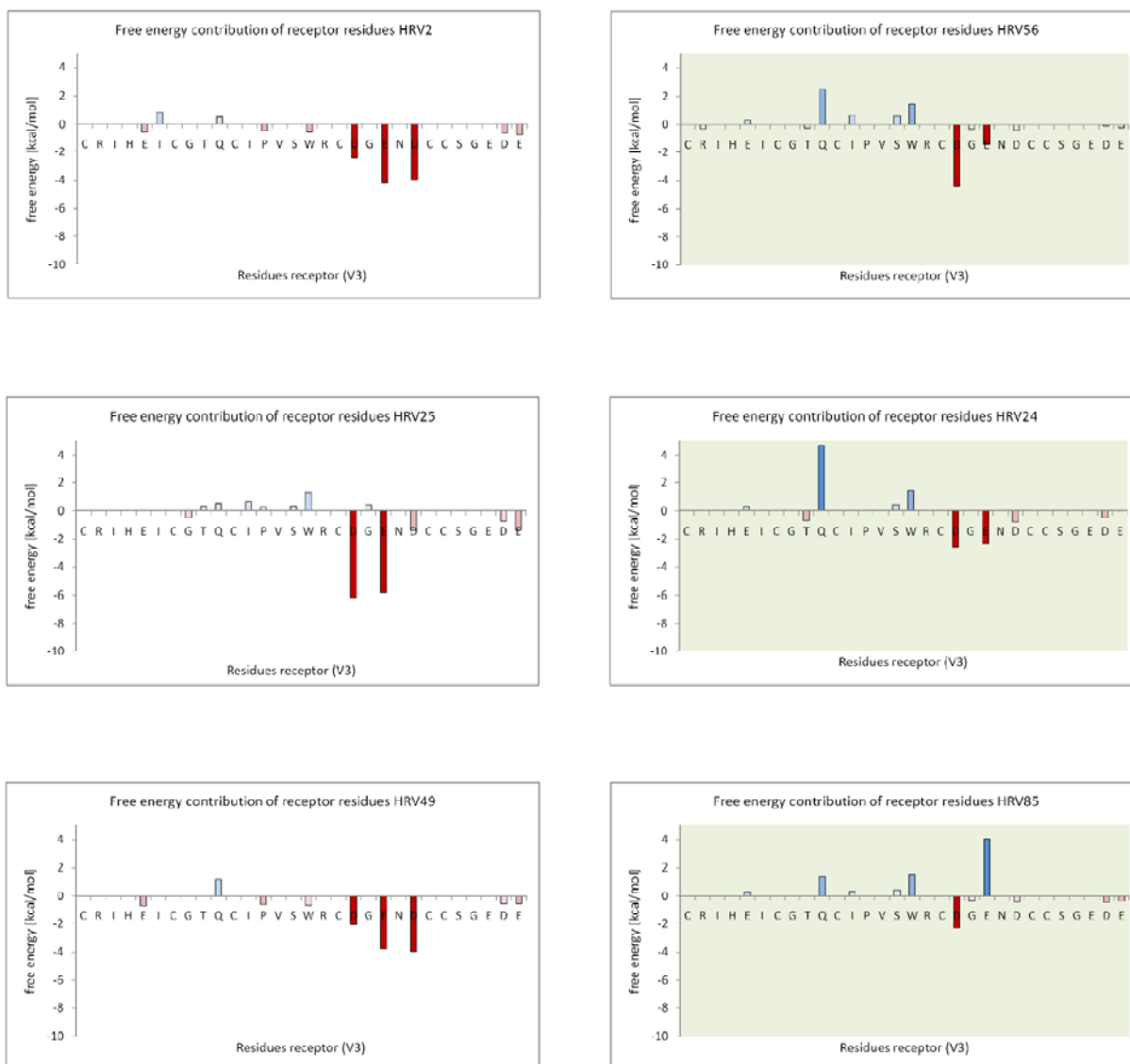


Figure 20: Bar diagrams depicting the interactions [kcal/mol] of the receptor residues (V3). Repulsive energies are colored in different shades of blue. Attractant energies are colored in different shades of red. Bar diagrams of K-type viruses have a green background color. Note that the presented energy values are a sum of all interactions at this receptor residue.

The summary table in Figure 21 shows the mean values of each receptor residue. Only energy contributions of a distinct receptor residue that are observed in more than 2 viruses of the same receptor group were considered in the analysis in Fig.21. K-type receptor interactions are colored green; minor group receptor interactions are colored blue. The error bars indicate the standard error of the mean. To assess whether the observed differences between minor and K-type viruses are statistically relevant, a statistical t-test (95%) was carried out. Significant differences were observed for 6 receptor residues. These receptor residues are marked with an asterisk. Summarizing the detected differences obtained by the heatmap and the receptor bar diagrams, interactions with acidic receptor residues are stronger for the minor group HRVs.

Also repulsive forces of the tryptophan in the receptor were much lower in the case of the minor group viruses.

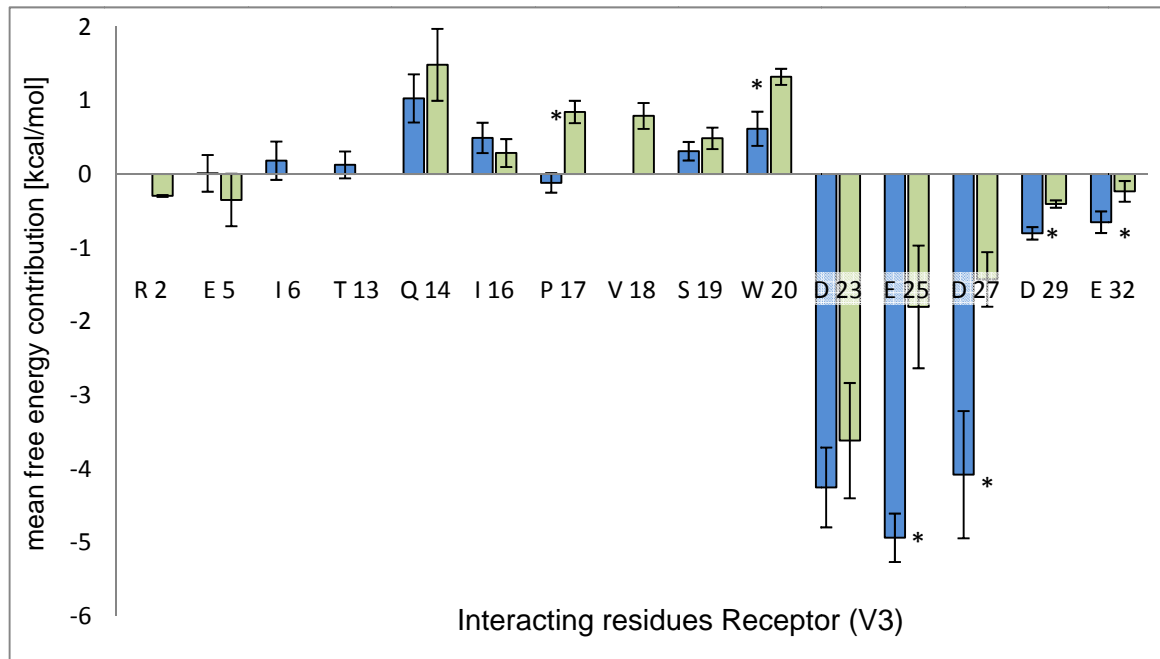


Figure 21: Mean free energy contribution of receptor residues in minor and K-Type viruses. The downward bars indicate negative energies at this position in the receptor. Interactions with positive free energy are presented with upward bars. The error bars represent the standard deviation of the mean (SEM). Asterisks indicate a significant difference at the confidence level of 95%.

4. Binding energies between HRVs and LDLR module 5 (L5) of human and mouse.

Although minor group rhinoviruses bind VLDLR very strongly, their natural receptors are LDLR and LRP. In particular, involvement of LDLR ligand binding repeat 5 (L5) in attachment of HRV1A and HRV2 was demonstrated [56]. Interestingly, HRV1A was found to strongly prefer the mouse receptor over its human homologue whereas HRV2 did not distinguish between the two. Therefore, the question arose whether this experimental finding would be reflected in the calculated binding energies.

Fortunately the structure of the extracellular domain of human LDL-receptor is available. [57]. So it was possible to build VP1-VP1* L5 (of human LDLR) complexes. The corresponding protein sequence of mouse L5 was found via sequence alignment with the human homolog. (See figure 22) The 3D structure of the mouse ligand binding repeat 5 was obtained by homology modeling via Swiss model. To obtain the same orientation of VLDLR

repeat 3 for LDLR repeat 5 of human and mouse, the structures were superimposed in *SPDBV* 3.7 using the iterative magic fit function. Once models of VP1-VP1* L5 (human/mouse) were produced their structure was energy minimized in *SPDBV* 3.7(100cycles). As the calculations with V3 of human VLDLR clearly indicated that Fastcontact gives the best result, the trimeric complexes were only submitted to this webserver.

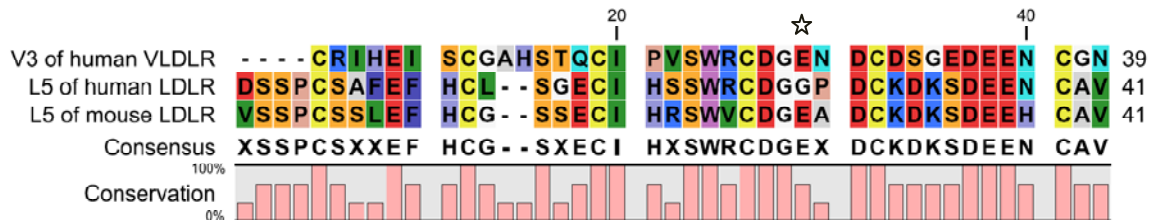


Figure 22: Alignment of human VLDL receptor repeat 3, L5 of human LDL receptor, and the murine homolog of L5. The percentage conservation is indicated as bar diagram below the alignment.

The L5 modules of human and mouse share 80% sequence identity. Whereas L5 (human and mouse) and V3 only share about 50% of the amino acid residues. However, the acidic clusters at the C-terminal end of receptor repeats are well conserved. Also the important tryptophan residue is fully conserved. The 3D structures of all 3 receptors are very similar. The similar folding of the 3 receptor fragments (V3, L5 human and L5 mouse) can be seen in Fig.23.

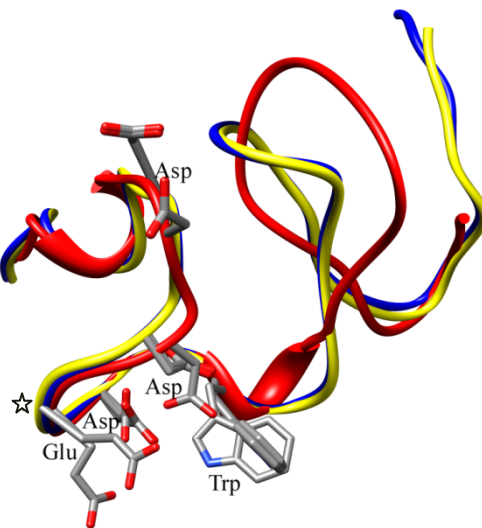


Figure 23: Structural comparison of V3 (red), human L5 (blue) and mouse L5 (yellow). No experimental structure of mouse L5 is known, thus we used a homology model. Most important residues for the interaction with virus VP1 are shown in stick representation. Note that human L5 does not possess a glutamic acid at position 30, which is an interaction partner of the strictly conserved lysine in the HI-loop. The position in the alignment and in the 3D structure is indicated with a black star.

4.1 Result of the Fastcontact calculations:

The replacement of the VLDLR repeat 3 through repeat 5 of LDLR or the mouse homolog respectively, revealed different binding affinities for some minor group viruses. The overall result using the mouse homolog of the LDLR ligand-repeat 5 instead of V3 (VLDLR) showed a similar performance regarding the separation of major and minor group viruses. (see Fig 24 M) It was possible to draw a separation line between major and minor group viruses. The only minor group virus type that showed a low binding affinity was HRV1B. In the case of the human L5(Fig.24 H), no clear separation of minor and major group viruses was obtained. The lowest affinities within the minor group viruses were calculated for HRV1A, HRV1B and HRV47.

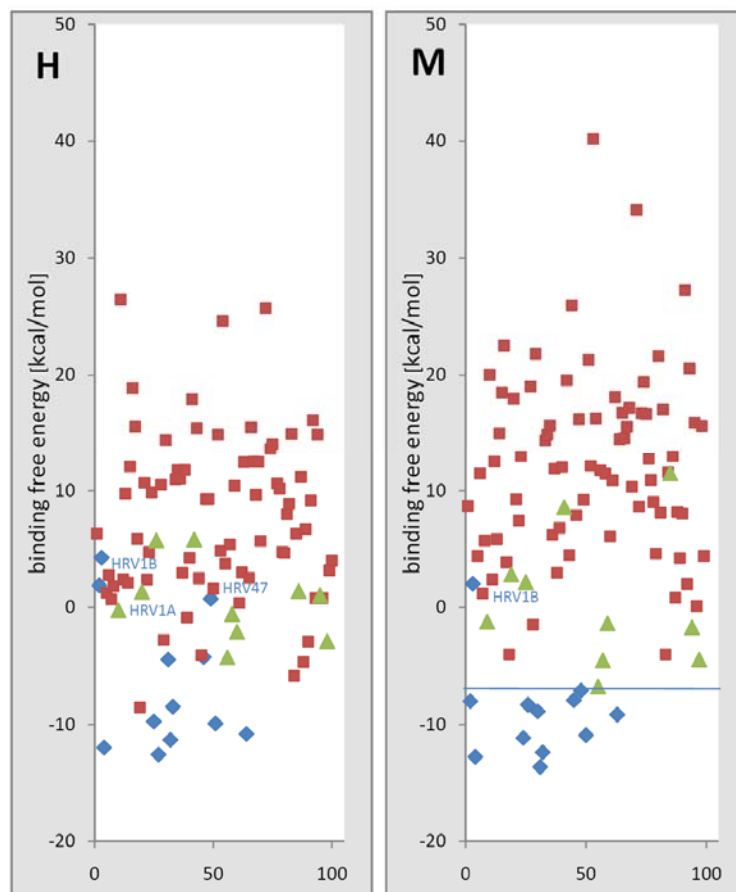


FIGURE 24: Calculated affinities of rhinoviruses for LDLR repeat 5 of mouse (M) and human (H). Note that the affinities of the minor group viruses (blue diamonds) and K-type (green diamonds) viruses were corrected with respect to the meaningless cysteine-interactions.

The low binding affinity of HRV1A to human L5 was proven by experimental approaches, see publication of Herdy [56]. According to her observations HRV1A strongly prefers the murine L5. This preference can be seen in Figure 28 M, where HRV1As calculated binding affinity was below the separation line. HRV1B shows low affinities for human and mouse

receptor repeat 5. These in-silico observations contradict the knowledge about the binding abilities of HRV1B. As a typical minor group virus HRV1B should be able to bind to the LDL receptor. Its ability to bind and infect mouse respiratory epithelial cells was shown in the work of Tuthill [58]. HRV47 is also predicted to have low affinity toward human LDLR L5 but this has not been shown experimentally. An explanation why HRV1B according to the energy calculations neither binds, the human L5 nor the mouse L5 with high affinities can be correlated with a bad 3D model of its VP1 loops. The fact that the protein sequence of HRV1B does not differ much from HRV1A, a minor group rhinovirus with already determined VP1 structure, weakens this argument. Furthermore, it is more likely that the quality of the 3D VP1 structure of HRV47 is rather low. Indication for this can also be seen in the results of the first calculations with V3, where HRV47 was predicted to have the lowest affinity to V3 of the VLDLR. Maybe also HRV47 has the same preference as HRV1A to the mouse homolog and does not bind the human LDLR. A possible reason why the human L5 does not support binding of rhinoviruses in excess, is that at position 30 the amino acid glycine is present. The other receptors possess in this position a glutamic acid (D25 in V3, D30 in mouse L5). This acidic residue is strongly involved in the virus receptor interaction (see Fig.19 and 21; especially pay attention to the energy contribution of E25). The favorable interaction partner of the glutamic acid is the conserved lysine in the HI-loop. (see heatmap in Fig.19) In contrast the glycine in human L5 is not able to interact with residues of the virus.

5. Bioinformatic analysis of the field isolated rhinoviruses:

5.1 Introduction:

Having shown the utility of this bioinformatic approach for the separation of minor group and K-type viruses we wanted to analyze 2 non classified rhinovirus field isolates. This was a great opportunity to assess the reliability of this bioinformatics approach.

These analyzed field isolates that were collected during a study about surveillance of enteroviruses in environmental specimens [59]. The study comprising data of 2001 to 2007, unclassified HRV field isolates were detected by using methods with optimized conditions for detecting enteroviruses, like poliovirus. Two of these unclassified HRV field samples are potentially interesting objects for studying the minor group receptor interactions, because a phylogenetic analysis revealed a close relationship to minor group viruses HRV1A and HRV1B. The fact which made these viruses even more interesting for our virus receptor interaction studies was that these sequences do not possess the strictly conserved lysine in the HI-loop that is a hallmark for minor group and K-type viruses. In the field isolates the lysine was replaced by an arginine. The question arose whether viruses possessing arginine instead of lysine can bind to LDLR family members. Site directed mutagenesis experiments, where the strictly conserved lysine was replaced by residues present at the same position in major group viruses, resulted in a lack of infectivity [60]. However, lysine has not been replaced by arginine so far. Arginine seems to be a proper substitute for lysine, as the basic character is maintained. Moreover, a similar interaction of an arginine residue in LDLA with the hemoglobin subunit b of lumbricus erythrocrucorin was observed [61]. Erythrocrucorin is an extracellular respiratory protein in the earthworm *lumbricus terrestris*. This protein is assembled from 180 polypeptide chains into an overall hexagonal bilayer shape. The interesting part of erythrocrucorin for us is the cysteine-rich LDL-A module that is homologous to the low-density lipoprotein (LDL) receptor. LDL-A modules interact with a hemoglobin b subunit in a similar way minor group rhinoviruses do. In this case the most involved amino acid is an arginine (Fig.25).

The sequences and virus samples we obtained from the author of the study[59].

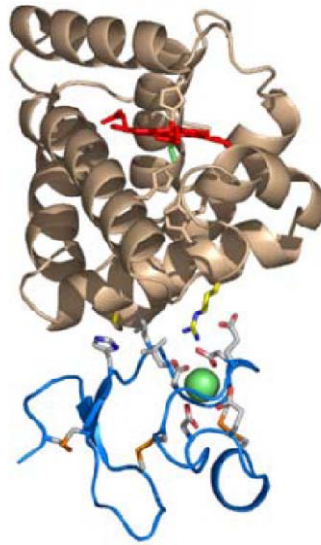


Figure 25: Interaction of the LDL-A part of lumbricus erythrocrucorin (blue) with a hemoglobin b subunit (brown). The calcium ion is colored in green and the 3 disulfide bonds are colored orange. The interacting arginine residue of the hemoglobin subunit b is colored in yellow. Illustration taken from the publication of Royer [61].

5.2 Bioinformatic affinity calculations:

The 2 VP1 sequences were treated in exactly the same way as the already classified one. For both field isolates HRV1A was selected by swissmodel as a template for modeling. This was not unexpected, because the 2 isolates share more than 92% protein-sequence identity with HRV1A. Thus, we can be sure that the predicted 3D structure is close to reality. For the energy calculation the online tool *Fastcontat 2.0* was used as before.

5.3 Results of the affinity calculations:

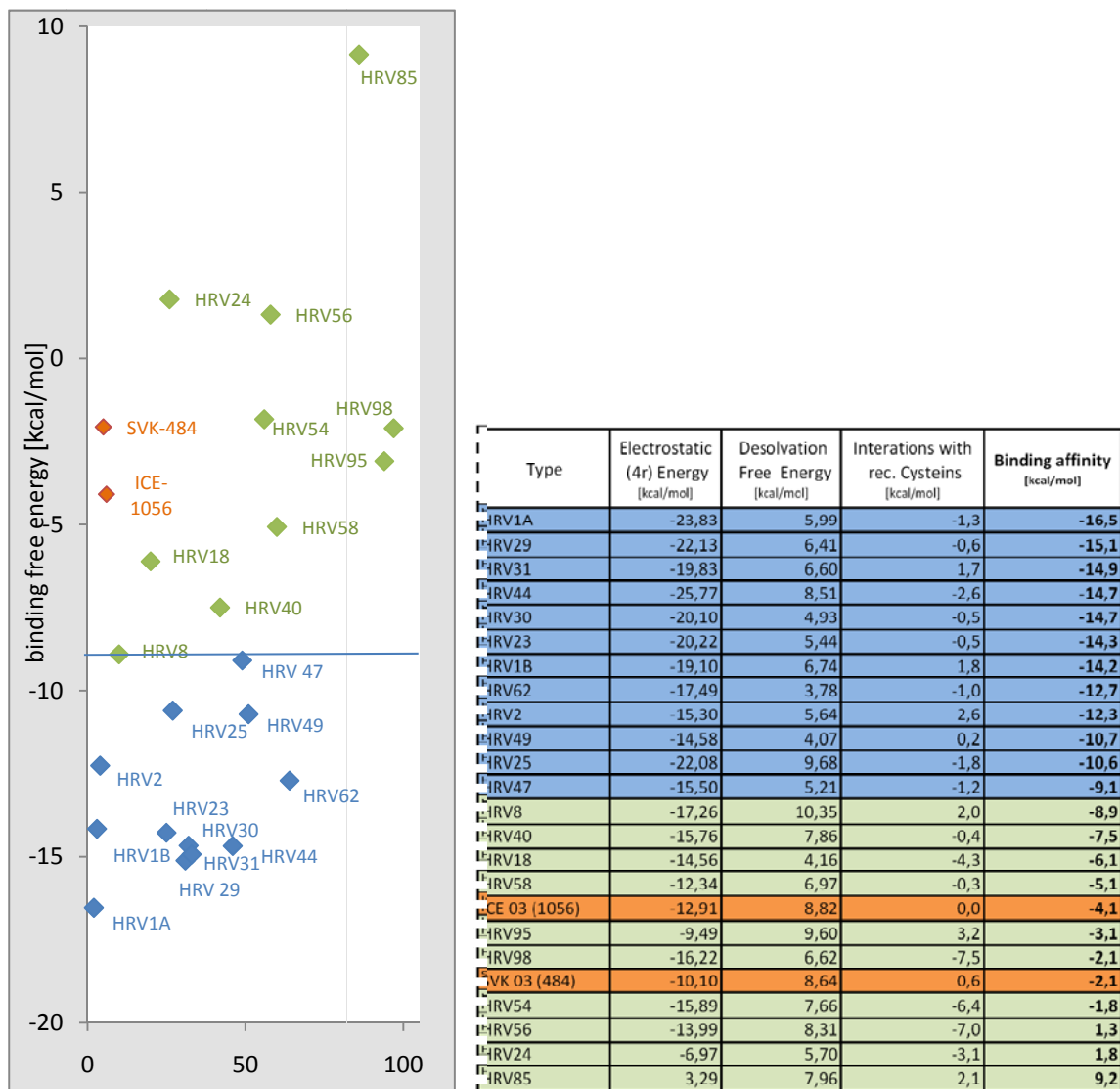


Figure 26: Energy table and diagram of the calculated binding affinities. The 2 field isolates are colored in orange. Minor group viruses are colored in blue; K-types in green.

According to the calculated affinities the 2 analyzed field isolates possess a major group character. Their receptor-binding affinities were much lower than that of minor group viruses. To answer the question about the reason for the weak binding abilities, the 10 best and 10 worst interacting residues were analyzed and represented in a heat map.

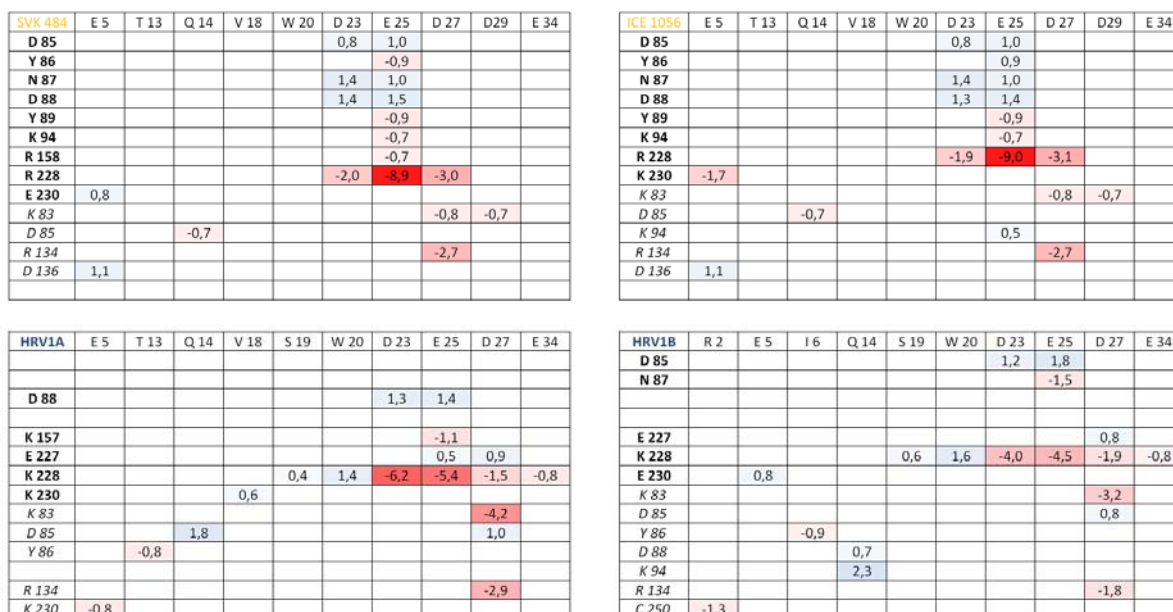


Figure 33: Heatmap representation of the 10 most repulsive and most attractive interactions. Receptor residues are written horizontally; VP1 residues vertically. VP1 residues from the first copy are in bold letters. Residues from the symmetry related copy are in italic. The values in the boxes represent the calculated energy (in kcal/mol) contribution of a distinct interaction of 2 amino acid residues.

Although the 2 field isolates do not differ much from HRV1A with respect to sequence, their calculated affinities and the binding pattern do. Whereas, only marginal differences between the 2 field isolates were found. In both field isolates, the highest attractant contribution of a single residue is found at the position 228 (arginine). The calculated interaction of this arginine 228 residue was surprisingly higher than the interaction of lysine 228 in HRV1A. The differences in the affinity cannot be explained by analyzing the 10 best and worst interactions using a heat map. For this reason another representation for displaying the interaction was used.

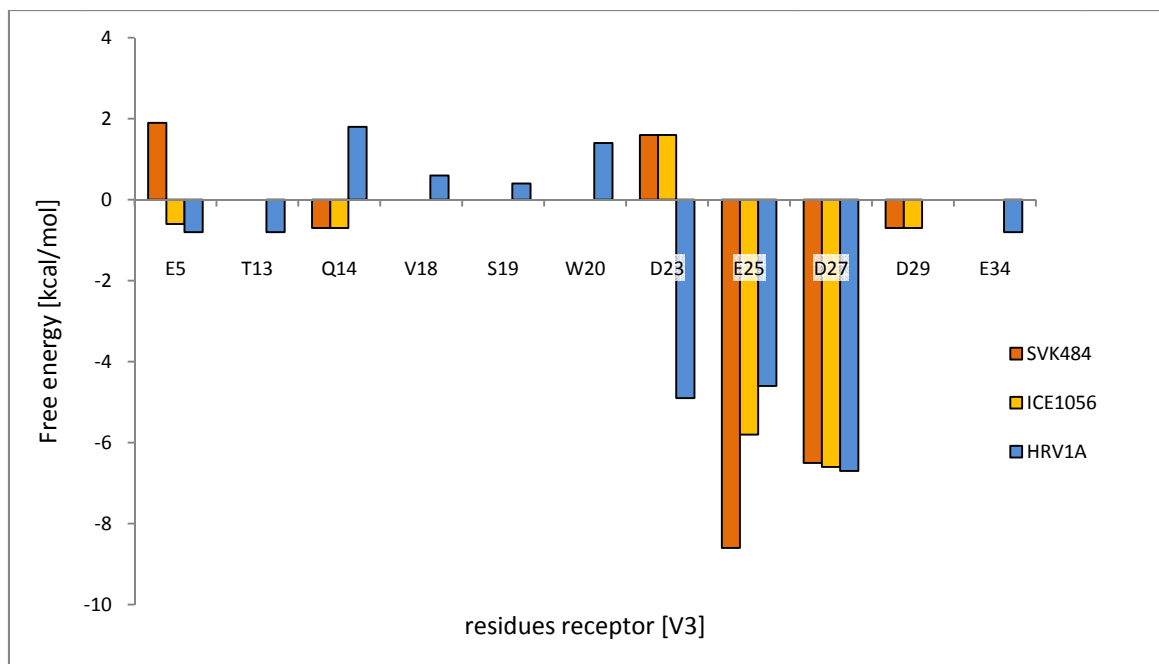


Figure 34: Sum of the energy contributions of the receptor residues of 2 field isolates and HRV1A. Repulsive interactions of receptor residues are represented in upward bars. The downward bars indicate residues in the receptor that are predicted to interact with residues of VP1 with negative free binding energy.

A proper representation that made it possible to recognize differences in the contribution of the binding involved amino acids, is a bar diagram with depicted energy values of the interacting receptor residues. Not dramatic differences were observed by analyzing Fig.34. Solely HRV1A shows a broader interaction with the acidic cluster of the receptor (D23-E34). The 2 field isolates do not interact with negative energy values with aspartic acid 23 (D23), whereas HRV1A did. SVK484 and ICE1056 did more or less behave the same. No specific reason for having lower affinity for VLDLR was found neither in the heat map nor in the bar diagram.

The low predicted affinities of the 2 field isolates were lower than those of MBP-V33333 binding K-types (i.e. HRV18 and HRV8). Therefore we set out to experimentally investigate the binding abilities of the field isolated rhinoviruses.

5.4 Detection of binding abilities of the field isolated viruses:

With this experiment we wanted to determine the binding abilities of the in-silico analyzed field isolated rhinoviruses. To assess the binding abilities a ligand binding blot was carried out.

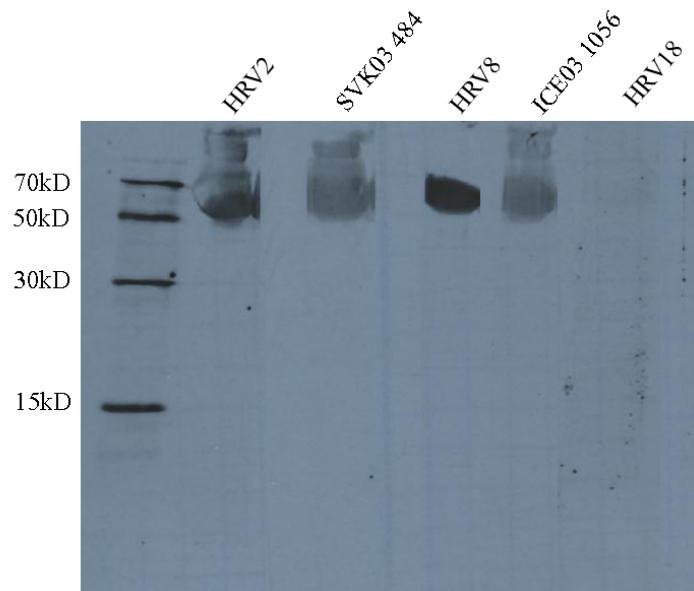


Figure 35: Ligand blot to detect binding of radiolabeled HRVs to MBP-V33333. Recombinant receptor was run on an SDS 10% polyacrylamide gel under non-reducing conditions and transferred to a PDV-membrane. Strips were incubated with 20,000 cpm each of ^{35}S -methionine labeled virus as indicated and exposed to X-ray film. HRV2, HRV18 and HRV8 were used as controls. HRV2 and HRV8 strongly bind to the receptor concatemer. HRV18 did not show any binding to MBP-V33333. The 2 examined field isolated rhinovirus types definitely bind to MBP-V33333, but not in such a great manner as the minor group virus HRV2 and the K-Type HRV8. This experiment was carried out by Irene Gösler.

The results of the ligand binding blot demonstrated that the isolated field isolates are able to bind the artificial receptor (MBP-V33333) weakly. When taking into account the in-silico predicted binding affinities, this ligand binding result contradicts the in-silico result. We also checked their abilities to infect cells lacking ICAM (RD cells). Notably all two field isolates were able to infect RD cells. Another important observation was that they grow equally well in RD and HeLa cells. Compared to the closely related (according to the VP1 sequence) minor group virus HRV1A, the viruses had a much longer infection time. We conclude that the two investigated field isolates do not use ICAM-1 as a receptor for cell entry and are therefore no major group viruses. Also we can say that a possible reason for the slow infection is that they do not efficiently bind the cellular receptor(s).

6. Mutational analysis of a major group human rhinovirus.

For the following experiments HRV14, the most extensively studied major group virus, was used. HRV14 belongs to the subgenus HRV-B. All B-types use ICAM-1 for cell entry while the small group of minor group viruses belong exclusively to the subgenus HRV-A. Another reason why we chose HRV14 was that its 3D structure is available [62]. Also, a full-length c-DNA clone of HRV14 in a vector with a T7 promoter is available [29,63]. This plasmid can be used for site directed mutagenesis; because of the T7 promoter, infectious RNA can be easily produced via *in-vitro* RNA transcription. The goal of this part of the project was to replace one of the 3 VP1 surface loops with that present in HRV2. The loops of VP1, building a star-shaped dome around the 5-fold axis of the virion, are called BC, DE and HI loop. The BC loop connects the second (B) with the third (C) strand within the typical β -barrel jelly-roll structure of VP1. In the case of the DE loop, strands D and E are connected.

For our experiments we picked the VP1 surface loop that contributes most to the receptor interaction; it connects the H-strand with the I-strand, and is therefore called HI-loop. When sequence alignments of all minor group viruses are taken into account, one single lysine residue within the HI-loop (K224 in HRV2) is strictly conserved. This lysine makes ionic interactions with an acidic cluster that is present in the ligand binding repeats of VLDLR. Ten members of the major group of HRVs also possess this strictly conserved lysine at an equivalent position in the middle of the HI loop. These latter HRVs infect cells via ICAM-1 and cannot use LDLR.

To obtain information about the structural basis of LDLR-binding we mutated the HI-loop of HRV14 in 2 different ways. From a structural point of view the HI-loops of HRV14 and HRV2 do not differ much from each other. However four amino-acid residues are different in the HI loops of HRV2 and HRV14 (Fig. 36). Once the mutated viruses are produced, their ability to bind LDLR can be checked via challenge of cells lacking endogenous ICAM-1 (e.g. human rhabdomyosarcoma cells) and testing for infectivity.

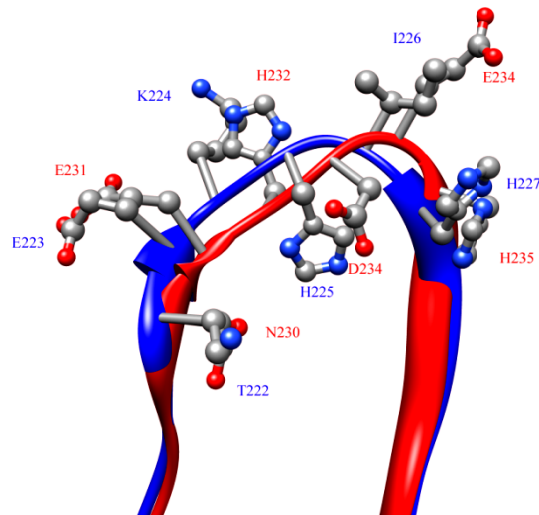


Figure 36: Structural comparison of the HI-loops of HRV14 (red) and HRV2 (blue). Figure created with UCSF Chimera [7].

6.1 PCR mutagenesis “round the horn”-method

The main goal of this project was to replace the HI loop sequence of HRV14 by the HI loop sequence of HRV2. The HI loop is located near the N terminus of VP1. It starts at residue 230 (HRV14) and comprises 6 amino acid-residues. To create a HRV14 HI loop chimera, PCR site directed mutagenesis was used. The plasmid pHRV14-as3f WT that contains the full genome of HRV14, served as a template. One of the primers carries the mutation that is flanked by 15 correctly base-paired nucleotides. The other primer is in reverse orientation, fully complement to the template sequence and much shorter. Successful PCR amplification results in a HI-loop-mutated linear plasmid. After ligation, the circular plasmid was amplified in *E. coli*. To confirm successful mutation and circularity, a restriction digest followed by agarose-gel electrophoresis was performed. The mutated plasmid should show exactly the same restriction pattern as the template plasmid. Obtaining a linear plasmid the unique *Acc65I* restriction site was used. Such a restriction is usually performed before the *in-vitro* transcription. For the other restriction reaction 2 unique restriction enzymes were used (*AvrII* and *KpnI*). No significant differences in size and restriction patterns were observed (Fig.37, left panel). After having verified the successful introduced mutations via sequencing, the clone was named HRV14_HI2 and used for *in-vitro* transcription.

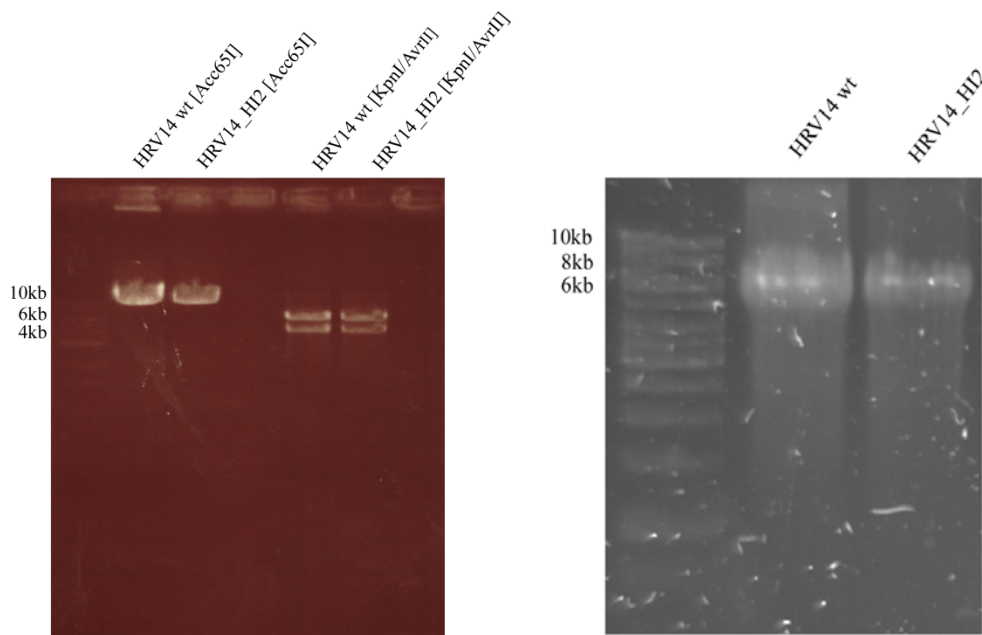


Figure 37. Left: Comparison of the restriction patterns via agarose gel-electrophoresis [1%] of the HRV14wt plasmid (HRV14-as3f WT) and the HRV14_HI2 plasmid after single-digestion with Acc65I (NEB) and double-digestion with KpnI/AvrII (NEB). Right: Agarose gel-electrophoresis [1%] of 1µg *in-vitro* transcribed RNA of HRV14 wt and HRV14_HI2.

6.2 *In-vitro* transcription of HRV14_HI2 RNA and transfection of HeLa cells.

For obtaining viral RNA that carries the desired mutation of the HI loop, the Ambion™ T7 *in-vitro* transcription kit was used. The *in-vitro* transcribed RNA was precipitated and its concentration was determined. The size of the RNA transcript was checked via agarose gel electrophoresis and compared to wild-type HRV14 RNA. No significant difference in the size of the transcripts was observed (Fig. 37, right panel). HeLa cells grown in 6 well plates were transfected with HRV14_HI2 RNA using magnetic bead assisted transfection (Matra). Unfortunately, transfection with HRV14_HI RNA did not result in infection-related cell death. Whereas a transfection of HRV14 WT RNA, that was used as a control resulted in CPE. Therefore, we had to find out whether the chimeric virus could eventually only accomplish one infection cycle. According to the work of Lee and colleagues [63] such virus can be identified via radiolabeling followed by SDS-PAGE and autoradiography. The procedure was performed as described in [63]. After the [³⁵S]-methionine/cysteine was added the infected cells were incubated for 24 h at 34°C. The radiolabelled viruses were pelleted via ultracentrifugation (70,000 rpm; 2 h). An aliquot of the dissolved virus particles was mixed with reducing SDS-buffer. The samples were heated to 95°C for 5 min and applied on a 15 % polyacrylamide gel. After separation of the proteins the gel was dried and exposed to a radiosensitive film (24h).

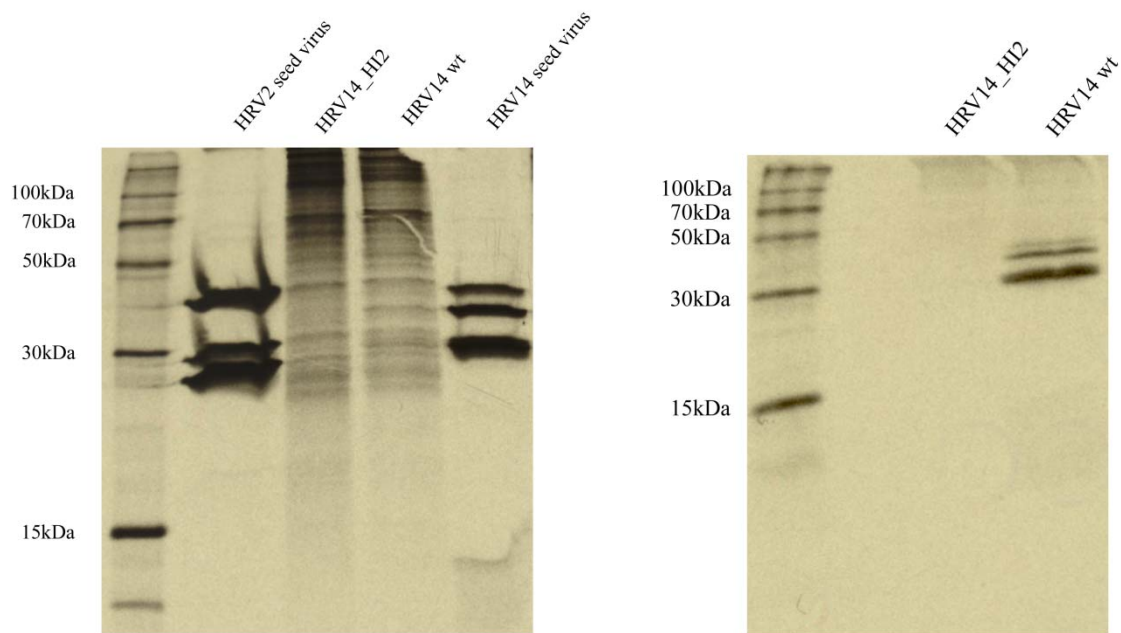


Figure 38: left ^{32}S radiolabelled virus samples. Samples were treated with reducing sample buffer and heated for 5 min at 95°C . ; right: Immune precipitated virus samples applied on a 15 % polyacrylamide gel under reducing conditions.

SDS-PAGE showed that a high virus concentration was required to see characteristic virus bands; the [^{35}S]-labeling only worked well when seed virus was used. This was the case for HRV2 and HRV14 (10^8 TCID₅₀). In samples transfected with the RNA no host protein shutoff was seen (left panel). To enrich the labeled virus particles, immune-precipitation was performed using α -HRV14 (rabbit) serum and staphylococcus aureus cells.

6.3 Immunoprecipitation of [^{35}S] labeled samples

Immune precipitation was performed using *Staphylococcus aureus* cells that were incubated with α -HRV14 (rabbit) serum. The *Staphylococcus aureus* cells with bound antibodies against HRV14 were washed twice and mixed with the radiolabelled virus samples. During incubation for 1h at RT the virus particles are bound by the antibody. Via centrifugation in an eppendorf centrifuge the *S. aureus* cells-antibody-virus particle complexes were separated from the non virus particles. The mixture was washed 3 times with RIPA buffer. After adding reducing SDS-buffer the samples were heated for 5 min to 95°C and applied on a polyacrylamidgel. Following the separation of the virus proteins via PAGE the gel was dried and exposed to a radiosensitive film.

With immunoprecipitation the radiolabelled virus particles were enriched. The typical bands representing the 3 structural proteins (VP1, VP2, VP3) were only detected in the wildtype

HR14 sample that was treated in the same way as the HRV14_HI chimera (Fig.38 right panel). This experiment demonstrated that the created HI-loop chimera of HRV14 is not infective.

6.4 PCR mutagenesis “quick change”

As the initially created chimeric virus seems to be non-infectious, we came to the conclusion that most probably additional mutations introduced by the polymerase during PCR amplification are the reason for the non-infectiveness. Excluding that the polymerase introduces to many errors, we used a polymerase with a higher fidelity.

The following experiments were carried out adhering to the protocol of “quick-change” without using the commercially available kit. In this method, 2 primers with exactly the same length are used. The part of the primer that carries the mismatch is located in the middle of the primer, flanked by 10-16 bases that are fully complementary to the template sequence. Compared to the method that was used before, the PCR reactions end up in a circular plasmid. There is no necessity for using phosphorylated primers and also the PCR subsequent ligation can be omitted. Also, a different PCR machine and a different DNA-polymerase were used; instead of Pfu (Promega®) the Phusion® (NEB®) polymerase. The performance of the Phusion® polymerase with respect to fidelity and speed is much better than that of Pfu.

By using this method, it was possible to create 2 different HRV14_HI chimeras. One named HRV14_K, which differs only in one amino acid from the wt sequence. The wildtype possesses, at position 3 in the HI loop, a histidine. The codon for the histidine (CAT) was changed into AAA, which is the codon for lysine. (Fig.39) The other HI loop chimera was again HRV14_HI2.

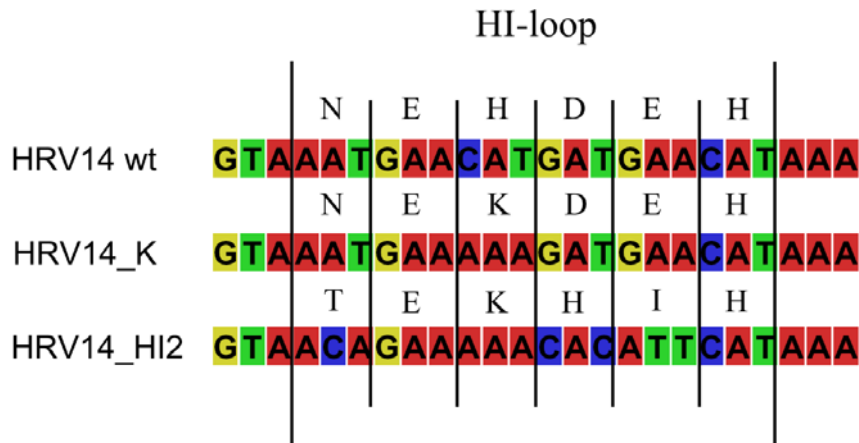


Figure 39: DNA and amino acid sequences of the 2 chimeric rhinoviruses in comparison to the HRV14 wt. The chimeric viruses only differ in this sequence, the rest of the sequence is identical to the wt HRV14 sequence.

6.5 RNA transcription and transfection of HeLa cells.

The mutated plasmids were linearized and *in-vitro* transcribed as described above. Virus RNA was precipitated with LiCl₂. The concentration of the RNA was determined and the size was verified on an agarose gel. As both were similar to that of the wt RNA it could be directly used for transfecting HeLa cells grown to 80% confluence by using Lipofectamine2000. After 2 days the cells were found to be lysed.

6.6 Screening the chimeric viruses via RT-PCR

Before the chimeric viruses were used for infection of RD cells, the loop region had to be sequenced, assuring that the introduced mutations were present in the viral RNA. To accomplish sequencing of the HI loop region of viral RNA, it first has to be transcribed into cDNA and amplified via PCR. Before reverse transcribing the viral RNA, the virus has to be separated from cell-debris and infection-medium via centrifugation and harvested via ultra-centrifugation. The virus pellet was dissolved in Tris-buffer (pH 8.5) and a 1 µl aliquot was taken for reverse transcription. The samples of the subsequent PCR reaction were sequenced confirming the correct introduction of a lysine in the RNA of HRV14_K; no mutation was detected in the RNA of HRV14_HI2. The loop sequence was identical to the wt sequence. However, sequencing of the HRV14_HI2 RNA that was used for transfection revealed that the sequence of the HI loop is mutated. To exclude that a contamination with wt HRV14 was responsible for this observation we repeated the transfection in HeLa and in RD-ICAM cells. In the virus samples of these transfections, again no mutation in the HI loop sequence was detected. This virus was thus not further considered.

6.7 Infection assay

The goal of this assay was to detect eventual differences in replication of HRV14_K and wt HRV14 upon infecting RD and RD-ICAM cells. The RD (human embryo rhabdomyosarcoma) cell line does not express ICAM-1. According to the hypothesis that a lysine at position 3 in the HI loop is one of the key players for the interaction with LDLR-family members, the chimeric rhinovirus HRV14_K might exhibit some, although low, affinity for LDL-receptors. However, it is not likely that HRV14_K can infect without using ICAM-1 as a receptor for cell entry. Infectivity of HRV14_K was compared to that of wt HRV14 in RD-ICAM cells. These cells are stably transfected to express human ICAM-1. Because of this they can be infected by minor group and major group rhinoviruses. The 80% confluent cell layers were incubated with serial dilutions of the supernatant of HRV14_K and HRV14 wt infected cells at 34°C for 3 days. Surviving cells were determined by crystal-violet staining (Fig. 40).

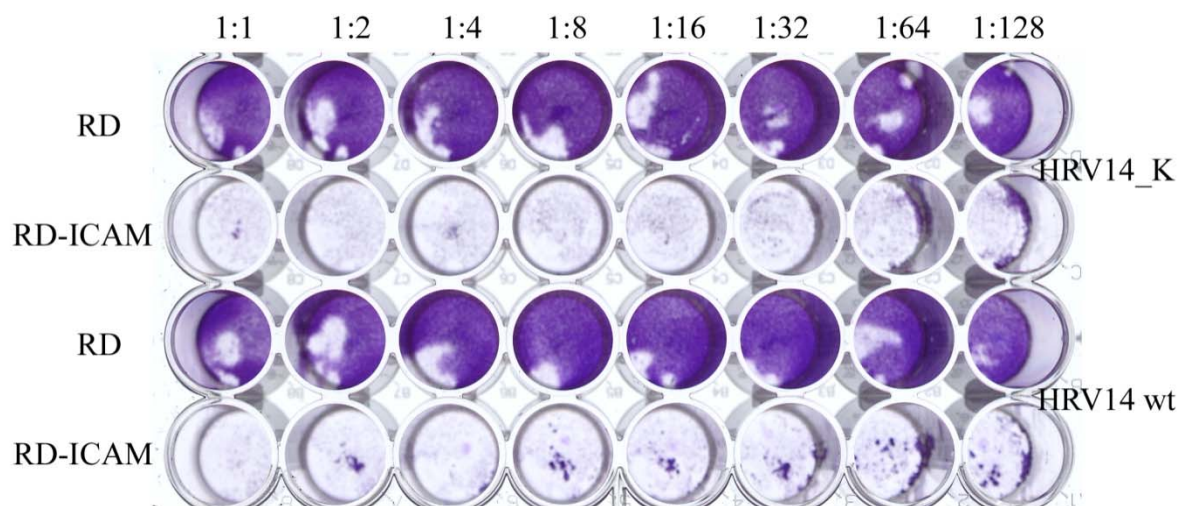


Figure 40: Result of the infectivity assay in RD and RD ICAM cells. The upper 2 rows were infected with HRV14_K supernatant in serial dilutions. The lower 2 rows were infected with HRV14 wt supernatant at the same dilutions.

As expected, no significant difference in infectivity between wt and HRV14_K was observed.

7. Discussion:

Bioinformatics:

The goal of this project was to find an easy automatable bioinformatic approach that is able from the basis of VP1 sequence data, to distinguish between major and minor group HRV's. Fortunately we found such a method that could distinguish between minor group and K-type viruses in silico.

The best result was obtained from the *Fastcontact* 2.0 web server. With this method it was possible to classify more than 80% of all minor group rhinoviruses correctly. With some improvements, i.e the correction of the not meaningfully cystein interactions of the receptor, the method was able to classify all minor group viruses correctly. As expected, the rhinoviruses with the second highest affinity to VLDLR, is the group of K-type viruses. The predictive power of the method is very good nevertheless the calculated affinity values are certainly not correct. The absolute values of HRV2 are far from those measured by fluorescence correlation spectroscopy [54]. Furthermore the highest affinity was calculated for HRV1A however, this contradicts the weak inhibition of infection with MBP-V33333 after 72 h of incubation, described in the publication of Verdaguer [33]. The K-type viruses that are described as weak binder of MBP-V33333 [Khan et al., unpulished], as HRV8 and HRV18 have calculated affinities that are close to the separation line. Having found a suitable method for affinity calculation, we also wanted to analyze the contribution of the involved residues of the different viruses. The primary goal was to find different conserved binding patterns in minor group and K-type viruses. Summarizing the results of the heat map and the bar diagram representations, we can say that there are no such defined patterns neither in K-types nor in minor group viruses. The same residues were found to contribute to binding in minor and K-type viruses, with only marginal differences. Nevertheless, the binding affinities to six receptor residues were higher for minor group viruses than for K-type viruses (statistically confirmed). Despite, all affinity predictions were based on models but not on experimentally determined structures the obtained results were remarkably good.

All calculations were based on the 3D structure of the HRV2 in complex with V3 of VLDLR. However VLDLR most probably does not play an important role for minor group virus cell entry, because it is not highly expressed in nasal epithelial cells, the primary site of rhinovirus infections.

We expected that the separation of minor and major group viruses based on the calculated affinities when using LDLR would be more clear cut. The results using the natural receptor (L5 of LDLR) substantially differ from the initial results. However the separation of minor and K-type viruses was much less clear, this may also be due to the use of two models (VP1-model and receptor model) that were superimposed to the HRV2/V3 structure.

All known minor group viruses share the same function as they all bind LDLR for cell entry. When we inspect the predicted binding affinities of all 12 minor group viruses to the ligand binding repeat 5 of human LDLR, it contradicts the known binding abilities of this virus group. A plausible reason, why this method could not reliably classify human rhinoviruses when the human LDLR (L5) was used as a receptor in the calculations is that this method was initially designed for predicting binding affinities to the V3 of VLDLR. The coordinates and exact orientation of the V3 were obtained from the determined structure in complex with HRV2 [33]. Down to the present day, no structure of a minor group virus in complex with a LDLR ligand repeat was published. Accordingly, we cannot be certain whether the orientation of virus and receptor corresponds to that adapted in real life. Furthermore, we cannot exclude that different minor group viruses use different ligand binding repeats for cell entry, or simply use ligand binding repeats of LRP.

Analysis of the unclassified field isolates.

This experiment was a great opportunity for evaluating our bioinformatic approach. Regardless of the close relationship between the field isolates to HRV1A, the 2 analyzed isolated types had much lower predicted affinities. Compared to affinities calculated for minor group viruses their affinities were much lower, suggesting that they probably cannot use LDLR. In this case the affinity calculation could not predict the right receptor specificity, since an infectivity test revealed that these viruses are able to replicate in cells without ICAM-1. In addition, a ligand binding blot showed that these viruses are able to weakly bind MBP-V33333.

To assess whether the arginine was the reason for decreased affinity, it was mutated to lysine in-silico and binding affinities were again calculated. The predicted binding affinities of this improved sequence (with the lysine) were approximately the same as the affinity of HRV2 (data not shown). This result suggests that the arginine residue within the HI-loop cannot strongly interact with the V3 of VLDLR, whereas a lysine residue can. We hypothesize that in contrast to K-type viruses the analyzed field isolates are able to uncoat at endosomal pH, and therefore are able to infect RD cells.

Mutagenesis:

The goal of this project was the creation of a HRV14 HI-loop chimeric virus. The wildtype HRV14 HI-loop sequence should be changed into the sequence of HRV2. At the end a HRV14 (major group) with the HI-loop sequence of HRV2 (minor group) should be established. The HI-loop is the most involved surface loop in the LDLR-rhinovirus interaction. The idea was that such a chimeric major group virus would have a greater affinity to the LDL receptor, a receptor that is not used by major group viruses. As the location of the mutations is structurally far away from the canyon, the ICAM-1 binding part of the virus capsid, it should not alter the binding to ICAM-1.

Since, no suitable restriction sites are present in the HRV14 genome that would allow an easy exchange of the HI-loop we had to use methods of site directed mutagenesis for the introduction of mutations. Generally larger plasmids, as the plasmid we were using (~10kb) are not easy to mutate. A general property of human rhinoviruses makes it even harder to mutate rhinovirus sequences, regarding the low G+C content (HRV14 VP1 36%). [11] The manuals of site directed mutagenesis kit always recommend the use of primers that have about 40% G-C content in their sequence. At first we used the method of “round the horn” site directed mutagenesis. With this method it was possible to introduce the full HI-loop of HRV2 into the sequence of HRV14 in one round of PCR amplification. The successfully introduced loop sequence was confirmed via DNA sequencing.

However, the RNA obtained upon transcription did not result in CPE in the transfected HeLa cells. Avoiding sequencing of the full rhinovirus genome, we decided to investigate whether the mutated virus RNA is able to at least initiate one round of infection. As this can be excluded the reason for the lack of replication is most probably correlated with polymerase induced errors in the RNA sequence. To overcome this problem a new method of site directed mutagenesis was carried out. With this method (“quick-change”), which utilizes a polymerase with higher accuracy, it was also possible to create the HRV14_HI2 chimera. At first the created chimera seems to be infective, but sequencing of RT PCR amplified virus cDNA revealed that the mutations cannot be found in virus samples. However, HRV14_K, a chimeric virus with only a slightly changed HI-loop that was also amplified with the “quick-change” method, was also tested for infectivity. It turned out that this chimeric virus was able to infect HeLa cells. The correct introduction of the mutation was confirmed via sequencing of the RT-PCR amplified viral cDNA. According to the result of an infectivity experiment, where RD and RD ICAM cells were challenged with HRV14_K and HRV14 wt viruses, no

significant differences between HRV14_K and HRV14 wt regarding infectivity could be observed.

Regardless of the used method, the chimeric viruses with the HRV2 HI-loop were not infective. It appears unlikely that the four changed amino-acid residues in the HI-loop are responsible for the loss of infectivity. This approach was designed to exchange residues that are important for interaction with LDL receptors, without changing the binding site (canyon) for the native receptor of major group rhinoviruses (ICAM-1). Therefore it can be excluded that mutation in the HI-loop alters the ICAM-1 binding site.

An explanation for the detection of wt sequences after transfection with HRV14_HI2 RNA could be that a non-homogenous RNA fraction of HRV14_HI2 was used for transfection. This in-homogenous RNA most probably contains traces of wt RNA that are not detected during sequencing. Excluding a real back-mutation of the HI-loop sequence after one round of infection suggests that the HRV14_HI2 clone is non-infectious. Otherwise the cDNA sequencing would have confirmed the mutation. Nevertheless the clone of HRV14_K is infective. This artificial K-Type does not differ from the HRV14 wildtype regarding infectivity, but it is an interesting object for later studies. Normal K-Type viruses are A class viruses and some of them are weak binders of MBP-V33333 (HRV8, HRV24, HRV18). This artificial one could help to answer the question whether B class viruses with a lysine in the HI loop can also bind MBP-V33333. The HRV14_K clone can be used for continuing with further mutagenesis experiments.

As a conclusion we can say that site directed mutagenesis can be used for mutating rhinovirus sequences. The reasons why the chimeric rhinovirus HRV14_HI2 is not infectious remains unclear.

References

- [1] Racaniello, V.R. and Baltimore, D. (1981). Cloned poliovirus complementary DNA is infectious in mammalian cells. *Science* 214, 916-9.
- [2] Whitton, J.L., Cornell, C.T. and Feuer, R. (2005). Host and virus determinants of picornavirus pathogenesis and tropism. *Nat Rev Microbiol* 3, 765-76.
- [3] Olson, N.H., Kolatkar, P.R., Oliveira, M.A., Cheng, R.H., Greve, J.M., McClelland, A., Baker, T.S. and Rossmann, M.G. (1993). Structure of a human rhinovirus complexed with its receptor molecule. *Proceedings of the National Academy of Sciences of the United States of America* 90, 507-511.
- [4] Price, W.H. (1956). The isolation of a new virus associated with respiratory clinical disease in humans. *Proc. Natl. Acad. Sci. U.S.A.* 42, 892-896.
- [5] W. Pelon, W.M., I. Philips et al. (1957). A cytopathic agent isolated from nasal recruits and mild respiratory illness. *Proc. Soc. Exp. Biol. Med.* 94, 262-267.
- [6] Kaiser, L. et al. (2006). Chronic rhinoviral infection in lung transplant recipients. *Am J Respir Crit Care Med* 174, 1392-9.
- [7] Pettersen, E.F., Goddard, T.D., Huang, C.C., Couch, G.S., Greenblatt, D.M., Meng, E.C. and Ferrin, T.E. (2004). UCSF Chimera--a visualization system for exploratory research and analysis. *J Comput Chem* 25, 1605-12.
- [8] Johnston, S.L. et al. (1995). Community study of role of viral infections in exacerbations of asthma in 9-11 year old children. *Bmj* 310, 1225-9.
- [9] Seemungal, T. et al. (2001). Respiratory viruses, symptoms, and inflammatory markers in acute exacerbations and stable chronic obstructive pulmonary disease. *Am J Respir Crit Care Med* 164, 1618-23.
- [10] Palmenberg, A.C., Spiro, D., Kuzmickas, R., Wang, S., Djikeng, A., Rathe, J.A., Fraser-Liggett, C.M. and Liggett, S.B. (2009). Sequencing and analyses of all known human rhinovirus genomes reveal structure and evolution. *Science* 324, 55-9.
- [11] Lau, S.K. et al. (2007). Clinical features and complete genome characterization of a distinct human rhinovirus (HRV) genetic cluster, probably representing a previously undetected HRV species, HRV-C, associated with acute respiratory illness in children. *J Clin Microbiol* 45, 3655-64.
- [12] McErlean, P., Shackelton, L.A., Andrews, E., Webster, D.R., Lambert, S.B., Nissen, M.D., Sloots, T.P. and Mackay, I.M. Distinguishing molecular features and clinical characteristics of a putative new rhinovirus species, human rhinovirus C (HRV C). *PLoS ONE*. 2008 Apr 2;3(4):e1847.
- [13] Dominguez, S.R. et al. Multiplex MasTag-PCR for respiratory pathogens in pediatric nasopharyngeal washes negative by conventional diagnostic testing shows a high prevalence of viruses belonging to a newly recognized rhinovirus clade. *J Clin Virol*. 2008 Oct;43(2):219-22.
- [14] Staunton, D.E., Merluzzi, V.J., Rothlein, R., Barton, R., Marlin, S.D. and Springer, T.A. (1989). A cell adhesion molecule, ICAM-1, is the major surface receptor for rhinoviruses. *Cell* 56, 849-53.
- [15] Hofer, F., Gruenberger, M., Kowalski, H., Machat, H., Huettinger, M., Kuechler, E. and Blaas, D. (1994). Members of the low density lipoprotein receptor family mediate cell entry of a minor-group common cold virus. *Proceedings of the National Academy of Sciences of the United States of America* 91, 1839-1842.
- [16] Rankl, C., Kienberger, F., Wildling, L., Wruss, J., Gruber, H.J., Blaas, D. and Hinterdorfer, P. (2008). Multiple receptors involved in human rhinovirus attachment to live cells. *Proc Natl Acad Sci U S A* 105, 17778-83.
- [17] Bella, J. and Rossmann, M.G. (1999). Review: rhinoviruses and their ICAM receptors. *J Struct Biol* 128, 69-74.

- [18] Bella, J. and Rossmann, M.G. (1999). Review: Rhinoviruses and their ICAM receptors. *Journal of Structural Biology* 128, 69-74.
- [19] Kolatkar, P.R., Bella, J., Olson, N.H., Bator, C.M., Baker, T.S. and Rossmann, M.G. (1999). Structural studies of two rhinovirus serotypes complexed with fragments of their cellular receptor. *Embo J* 18, 6249-59.
- [20] Rueckert, R.R. (1996) Picornaviridae: The Viruses and Their Replication. In *Fields Virology* (Fields, B.N., Kipe, D.M. and Howley, P.M., ed. eds), pp. 609-654. Lippincott - Raven Publishers, Philadelphia.
- [21] Rossmann, M.G. (1989). The canyon hypothesis - Hiding the host cell receptor attachment site on a viral surface from immune surveillance. *Influence of Molecular Biology on Drug Discovery* 1, 56-65.
- [22] Smith, T.J. et al. (1993). Structure of human rhinovirus complexed with Fab fragments from a neutralizing antibody. *J Virol* 67, 1148-1158.
- [23] Mosser, A.G., Shepard, D.A. and Rueckert, R.R. (1994). Use of drug-resistance mutants to identify functional regions in picornavirus capsid proteins. *Arch Virol Suppl* 9, 111-9.
- [24] Andersen, O.M. and Petersen, H.H. (2003). New light on a long-known protein family. *Chembiochem* 4, 1137-46.
- [25] Nicodemou, A., Petsch, M., Konecni, T., Kremser, L., Kenndler, E., Casasnovas, J.M. and Blaas, D. (2005). Rhinovirus-stabilizing activity of artificial VLDL-receptor variants defines a new mechanism for virus neutralization by soluble receptors. *FEBS Lett* 579, 5507-5511.
- [26] Rebeck, G.W., LaDu, M.J., Estus, S., Bu, G. and Weeber, E.J. (2006). The generation and function of soluble apoE receptors in the CNS. *Mol Neurodegener* 1, 15.
- [27] Tumova, S., Woods, A. and Couchman, J.R. (2000). Heparan sulfate proteoglycans on the cell surface: versatile coordinators of cellular functions. *Int J Biochem Cell Biol* 32, 269-288.
- [28] Khan, A.G., Pichler, J., Rosemann, A. and Blaas, D. (2007). Human Rhinovirus Type 54 Infection via Heparan Sulfate is Less Efficient and Strictly Dependent on the Low Endosomal pH.
- [29] Skern, T., Torgersen, H., Auer, H., Kuechler, E. and Blaas, D. (1991). Human rhinovirus mutants resistant to low pH. *Virology* 183, 757-63.
- [30] Breslauer, K.J., Frank, R., Blocker, H. and Marky, L.A. (1986). Predicting DNA duplex stability from the base sequence. *Proc Natl Acad Sci U S A* 83, 3746-50.
- [31] Hewat, E.A., Neumann, E., Conway, J.F., Moser, R., Ronacher, B., Marlovits, T.C. and Blaas, D. (2000). The cellular receptor to human rhinovirus 2 binds around the 5-fold axis and not in the canyon: a structural view. *Embo J* 19, 6317-6325.
- [32] Baranowski, E., Sevilla, N., Verdaguer, N., RuizJarabo, C.M., Beck, E. and Domingo, E. (1998). Multiple virulence determinants of foot-and-mouth disease virus in cell culture. *Journal Of Virology* 72, 6362-6372.
- [33] Verdaguer, N., Fita, I., Reithmayer, M., Moser, R. and Blaas, D. (2004). X-ray structure of a minor group human rhinovirus bound to a fragment of its cellular receptor protein. *Nature Struct. Mol. Biol.* 11, 429-434.
- [34] Crump, C.E., Arruda, E. and Hayden, F.G. (1993). In vitro inhibitory activity of soluble ICAM-1 for the numbered serotypes of human rhinovirus. *Antiviral Chemistry & Chemotherapy* 4, 323-327.
- [35] Uncapher, C.R., Dewitt, C.M. and Colonna, R.J. (1991). The major and minor group receptor families contain all but one human rhinovirus serotype. *Virology* 180, 814-817.
- [36] Querol-Audi, J., Konecni, T., Pous, J., Carugo, O., Fita, I., Verdaguer, N. and Blaas, D. (2009). Minor group human rhinovirus-receptor interactions: geometry of multimodular attachment and basis of recognition. *FEBS Lett* 583, 235-40.
- [37] Chothia, C. (1992). Proteins. One thousand families for the molecular biologist. *Nature* 357, 543-4.

- [38] Ledford, R.M., Patel, N.R., Demenczuk, T.M., Watanyar, A., Herbertz, T., Collett, M.S. and Pevear, D.C. (2004). VP1 sequencing of all human rhinovirus serotypes: Insights into genus phylogeny and susceptibility to antiviral capsid-binding compounds. *J Virol* 78, 3663-3674.
- [39] Blomqvist, S., Savolainen, C., Raman, L., Roivainen, M. and Hovi, T. (2002). Human rhinovirus 87 and enterovirus 68 represent a unique serotype with rhinovirus and enterovirus features. *J Clin Microbiol* 40, 4218-4223.
- [40] Schwede, T., Kopp, J., Guex, N. and Peitsch, M.C. (2003). SWISS-MODEL: an automated protein homology-modeling server. *Nucleic Acids Res* 31, 3381-3385.
- [41] Guex, N. and Peitsch, M.C. (1997). SWISS-MODEL and the Swiss-PdbViewer: an environment for comparative protein modeling. *Electrophoresis* 18, 2714-2723.
- [42] Laine, P., Blomqvist, S., Savolainen, C., Andries, K. and Hovi, T. (2006). Alignment of capsid protein VP1 sequences of all human rhinovirus prototype strains: conserved motifs and functional domains. *J Gen Virol* 87, 129-138.
- [43] Hadfield, A.T. et al. (1995). Structural studies on human rhinovirus 14 drug-resistant compensation mutants. *J Mol Biol* 253, 61-73.
- [44] Silberstein, E., Dveksler, G. and Kaplan, G.G. (2001). Neutralization of hepatitis A virus (HAV) by an immunoadhesin containing the cysteine-rich region of HAV cellular receptor-1 [In Process Citation]. *J Virol* 75, 717-25.
- [45] Carrillo-Tripp, M. et al. (2009). VIPERdb2: an enhanced and web API enabled relational database for structural virology. *Nucleic Acids Res* 37, D436-42.
- [46] W. F. van Gunsteren, S.R.B., A. A. Eising, P. H. Hünenberger, and P. Krüger, A.E.M., W. R. P. Scott, and I. G. Tironi. . (1996). Biomolecular Simulation: GROMOS96 Manual and User Guide. BIOMOS b.v., Zürich, Groningen, 1996.
- [47] Zhou, H., Zhang, C., Liu, S. and Zhou, Y. (2005). Web-based toolkits for topology prediction of transmembrane helical proteins, fold recognition, structure and binding scoring, folding-kinetics analysis and comparative analysis of domain combinations. *Nucleic Acids Res* 33, W193-7.
- [48] Champ, P.C. and Camacho, C.J. (2007). FastContact: a free energy scoring tool for protein-protein complex structures. *Nucleic Acids Res* 35, W556-60.
- [49] Camacho, C.J. and Zhang, C. (2005). FastContact: rapid estimate of contact and binding free energies. *Bioinformatics* 21, 2534-6.
- [50] Vlasak, M., Roivainen, M., Reithmayer, M., Goesler, I., Laine, P., Snyers, L., Hovi, T. and Blaas, D. (2005). The minor receptor group of human rhinovirus (HRV) includes HRV23 and HRV25, but the presence of a lysine in the VP1 HI loop is not sufficient for receptor binding. *J Virol* 79, 7389-7395.
- [51] Petrey, D. and Honig, B. (2003). GRASP2: visualization, surface properties, and electrostatics of macromolecular structures and sequences. *Methods Enzymol* 374, 492-509.
- [52] Bieri, S., Djordjevic, J.T., Daly, N.L., Smith, R. and Kroon, P.A. (1995). Disulfide bridges of a cysteine-rich repeat of the LDL receptor ligand-binding domain. *Biochemistry* 34, 13059-13065.
- [53] Nizet, S., Wruss, J., Landstetter, N., Snyers, L. and Blaas, D. (2005). A mutation in the first ligand-binding repeat of the human very-low-density lipoprotein receptor results in high-affinity binding of the single V1 module to human rhinovirus 2. *J Virol* 79, 14730-14736.
- [54] Wruss, J., Rünzler, D., Steiger, C., Chiba, P., Köhler, G. and Blaas, D. (2007). Attachment of VLDL-Receptors to an Icosahedral Virus along the five-fold Symmetry Axis: Multiple Binding Modes Evidenced by Fluorescence Correlation Spectroscopy. *Biochemistry*
- [55] Ronacher, B., Marlovits, T.C., Moser, R. and Blaas, D. (2000). Expression and folding of human very-low-density lipoprotein receptor fragments: neutralization capacity toward human rhinovirus HRV2. *Virology* 278, 541-550.
- [56] Herdy, B., Snyers, L., Reithmayer, M., Hinterdorfer, P. and Blaas, D. (2004). Identification of the human rhinovirus serotype 1A binding site on the murine low-density lipoprotein receptor by using human-mouse receptor chimeras. *J Virol* 78, 6766-6774.

- [57] Rudenko, G., Henry, L., Henderson, K., Ichtchenko, K., Brown, M.S., Goldstein, J.L. and Deisenhofer, J. (2002). Structure of the LDL receptor extracellular domain at endosomal pH. *Science* 298, 2353-8.
- [58] Tuthill, T.J. et al. (2003). Mouse respiratory epithelial cells support efficient replication of human rhinovirus. *J Gen Virol* 84, 2829-36.
- [59] Blomqvist, S., Savolainen-Kopra, C., Paananen, A., Hovi, T. and Roivainen, M. (2009). Molecular characterization of human rhinovirus field strains isolated during surveillance of enteroviruses. *J Gen Virol*
- [60] Duechler, M., Ketter, S., Skern, T., Kuechler, E. and Blaas, D. (1993). Rhinoviral receptor discrimination: mutational changes in the canyon regions of human rhinovirus types 2 and 14 indicate a different site of interaction. *J Gen Virol* 74, 2287-2291.
- [61] Royer, W.E., Jr., Sharma, H., Strand, K., Knapp, J.E. and Bhyravbhatla, B. (2006). Lumbricus erythrocyruorin at 3.5 Å resolution: architecture of a megadalton respiratory complex. *Structure* 14, 1167-77.
- [62] Rossmann, M.G. et al. (1985). Structure of a human common cold virus and functional relationship to other picornaviruses. *Nature* 317, 145-53.
- [63] Lee, W.M., Monroe, S.S. and Rueckert, R.R. (1993). Role of maturation cleavage in infectivity of picornaviruses: activation of an infectosome. *J Virol* 67, 2110-2122.

Acknowledgement:

In the first place I want to thank professor Dieter Blaas that he gave me the chance to do my diploma thesis in his lab. Dieter is having an inexhaustible reservoir of ideas to overcome a scientific problem. The lab I was working for about a year was quite small, but full of intelligent and motivated people, who never hesitated to help when I had a question. In detail I want to thank Angela for being my supervisor. Gerhard for broaden my horizons concerning computers and software. Victor for being an example of carefulness and exactness in almost everything he does. I also want to thank Abdul for teaching me how to do different techniques right in the lab and as well I want to thank him for fruitful discussions about my obtained results. A special thank goes to Irene, she is really enrichment for this lab. Irene always had the right answer for my questions. She also performed 2 experiments that are presented in this work, once again thanks for that. I hope I could learn a little bit from all of you during my time to in the Blaas lab, to become one day a good scientist as well. I also want to thank my girlfriend Sophie for being a good support when things in the lab didn't work out as they should. Finally I want to thank my family for supporting me financially and emotionally during the long time of university study.

Curriculum vitae

name: Weber Christoph

born: 26. Juli 1983

nationality: Austria

address: Pframa 8
2305 Eckartsau

email: a0307431@unet.univie.ac.at
christoph.weber@univie.ac.at

education:

1989 – 1993	Volksschule 2304 Orth an der Donau
1993 – 1997	Hauptschule 2304 Orth an der Donau
1997 – 2002	HLBLA Francisco Josephinum 3250 Wieselburg
06. 2002	final exams (Matura)
since 10. 2003	Study of Biology (Microbiology and Genetics) <i>University of Vienna</i>

working experiences:

2007	2 month internship at Baxter (Orth a/d Donau)
since 5. 2008	Diploma thesis in the group of Prof. Dr. Dieter Blaas at the MFPL (Max F. Perutz Laboratories)